Neuronal Remodeling During Metamorphosis Is Regulated by the *alan shepard* (*shep*) Gene in *Drosophila melanogaster*

Dahong Chen,* Chunjing Qu,*,[1] Sonia M. Bjorum,[†,2] Kathleen M. Beckingham,[†] and Randall S. Hewes*,[3]
*Department of Biology, University of Oklahoma, Norman, Oklahoma 73019, and
[†]Department of Biochemistry and Cell Biology, Rice University, Houston, Texas 77005
ORCID IDs: 0000-0003-4403-6788 (D.C.); 0000-0002-7518-7215 (R.H.)

ABSTRACT Peptidergic neurons are a group of neuronal cells that synthesize and secrete peptides to regulate a variety of biological processes. To identify genes controlling the development and function of peptidergic neurons, we conducted a screen of 545 splice-trap lines and identified 28 loci that drove expression in peptidergic neurons when crossed to a GFP reporter transgene. Among these lines, an insertion in the *alan shepard* (*shep*) gene drove expression specifically in most peptidergic neurons. *shep* transcripts and SHEP proteins were detected primarily and broadly in the central nervous system (CNS) in embryos, and this expression continued into the adult stage. Loss of *shep* resulted in late pupal lethality, reduced adult life span, wing expansion defects, uncoordinated adult locomotor activities, rejection of males by virgin females, and reduced neuropil area and reduced levels of multiple presynaptic markers throughout the adult CNS. Examination of the bursicon neurons in *shep* mutant pharate adults revealed smaller somata and fewer axonal branches and boutons, and all of these cellular phenotypes were fully rescued by expression of the most abundant wild-type *shep* isoform. In contrast to *shep* mutant animals at the pharate adult stage, *shep* mutant larvae displayed normal bursicon neuron morphologies. Similarly, *shep* mutant adults were uncoordinated and weak, while *shep* mutant larvae displayed largely, although not entirely, normal locomotor behavior. Thus, *shep* played an important role in the metamorphic development of many neurons.

PEPTIDERGIC neurons produce small peptides, called neuropeptides, which are secreted within the nervous system to influence the activity of other neurons or into the blood to act on other tissues. Through these targets, neuropeptides regulate a wide range of processes, which include development, feeding, growth, aggression, reproduction, and learning and memory (McShane *et al.* 1992; Park *et al.* 2003; Luquet *et al.* 2005; Crown *et al.* 2007; Nephew *et al.* 2009; Slaidina *et al.* 2009; Goncalves *et al.* 2012).

One of the first genes identified to play a specific role in the development of peptidergic neurons was *dimmed* (*dimm*), which encodes a basic helix–loop–helix transcription factor that is required for the differentiation of diverse peptidergic neurons (Hewes *et al.* 2003; Park *et al.* 2008; Hamanaka *et al.* 2010). DIMM is a key regulator of expression of the neuropeptide biosynthetic enzyme, peptidylglycine-α-hydroxylating monooxygenase (PHM) (Park *et al.* 2008), and it promotes the differentiation of neurosecretory properties in many neurons (Hamanaka *et al.* 2010). Both DIMM and PHM are expressed widely and specifically in peptidergic neurons (Acampora *et al.* 1999; Michaud *et al.* 1998; Jiang *et al.* 2000; Hewes *et al.* 2003). In fact, DIMM was first identified by virtue of its pattern of peptidergic neuron expression through an enhancer-trap screen (Hewes *et al.* 2003). Similar expression pattern-based strategies may be useful for identification of other factors critical for peptidergic neuron development.

In this study, we sought to identify similar factors through a splice-trap screen for genes with peptidergic cell-specific expression patterns. We identified 28 insertions with different patterns of peptidergic cell reporter gene expression, driven by *P*-element splice-trap insertions in specific loci. These insertions drove reporter expression in insulin-like

doi: 10.1534/genetics.114.166181
Manuscript received May 15, 2014; accepted for publication June 5, 2014; published Early Online June 13, 2014.
Supporting information is available online at http://www.genetics.org/lookup/suppl/doi:10.1534/genetics.114.166181/-/DC1.
Sequence data have been deposited with the EMBL/GenBank Data Libraries under accession nos. NM002898, NM001086938, EHB06530, NP001020574, NP062685, NM001002172, AAA69698, FBpp0288676, FBpp0112400, NP001410.
[1]Present address: Baylor College of Medicine, Houston, Texas 77030.
[2]Present address: American Type Culture Collection, Manassas, VA 20110.
[3]Corresponding author: Department of Biology, University of Oklahoma, 730 Van Vleet Oval, Rm. 314, Norman, OK 73019. E-mail: hewes@ou.edu

peptide 2 (ILP2), crustacean cardioactive peptide (CCAP)/bursicon, -RFamide, Furin 1, and leucokinin (LK) cells and often caused defects typical of disrupted neuropeptide signaling. Thus, all 28 of these genes are strong candidate regulators of peptidergic cell development or function.

We mapped one of the splice-trap insertions to an exon of the *alan shepard* (*shep*) gene (Bjorum 2006), and we chose this insertion for further analysis because it displayed an expression pattern that was highly similar to PHM and DIMM. *shep in situ* hybridization and anti-SHEP immunostaining later revealed that both the *shep* mRNA and SHEP protein expression is enriched in most neurons, yet *shep* mutants displayed defects in adult eclosion and wing expansion that suggested specific disruptions in signaling by bursicon and other neuropeptides. Consistent with these behavioral phenotypes, the *shep* mutant bursicon neurons had smaller somata, fewer axon branches, and smaller and fewer neuroendocrine boutons, and all of these phenotypes were rescued by expression of a wild-type *shep* cDNA. Interestingly, pan-neuronal RNA interference to *shep* produced smaller CNS neuropils and defects in general locomotor behaviors, such as flipping and climbing. Most of the locomotor phenotypes were restricted to the adult stage, and the effects of *shep* mutations on neuronal growth were restricted to pupal development. Thus, *shep* regulates metamorphic growth of the bursicon neurons, and it may also serve as a general regulator of neuronal growth during metamorphic remodeling.

Materials and Methods

Stocks

Drosophila melanogaster stocks and crosses were cultured on standard cornmeal–yeast–agar media at 25°. We obtained splice-trap strains, deficiency strains, and *Gal4* strains from the Bloomington *Drosophila* Stock Center. We used three *shep* deficiencies: *Df(3L)ED210* (FBab0035327), *Df(3L)Exel6104* (FBab0038124), and *Df(3L)Exel6103* (FBab0038123). The *Gal4* lines used were *386–Gal4* (FBti0020938) (Bantignies *et al.* 2000), *en–Gal4* (Fox *et al.* 2010), *D42–Gal4* (Yeh *et al.* 1995), *elav–Gal4* (FBti0002575) (Shakiryanova *et al.* 2005), and *ccap–Gal4* (FBti0037998) (Park *et al.* 2003). The *UAS–shep-RNAi* stock was obtained from the Vienna *Drosophila* RNAi Center (*w*^{1118}; *P{GD5125}v37863:* FBst0462204).

EST sequence verification

We randomly selected six *shep* EST clones that shared the 5′ end represented by isoforms *shep-RE* (RE), *shep-RH* (RH), and *shep-RI* (RI) and amplified them with forward primer 5′-GCCGAATTCTGAGCAACACGACGAACAC-3′ and reverse primer 5′-CGCAGATCTTGGCTTTTCCGCTTCTC-3′. Subsequent sequencing of each EST clone for the RE isoform-specific sequence CAACAG in exon 13 (FBgn0052423:13) was performed with the forward primer to distinguish RE from RH and RI.

UAS–shep

A *shep–RE/RG* isoform cDNA was generated from a male wild-type fly (*Oregon R*) by RT–PCR with forward primer 5′-GCCGAATTCTGAGCAACACGACGAACAC-3′ and reverse primer 5′- CGCAGATCTTGGCTTTTCCGCTTCTC-3′. The cDNA was inserted into pUAST between the *Eco*RI and *Bgl*II sites in the polylinker and transformed into DH5α *Escherichea coli*, and a single transformant colony was selected for sequence verification. The forward primer 5′-GCCGAATTCT GAGCAACACGACGAACAC-3′ was used to check for the sequence GTGGGTATCTGGGTGCTTCATAGGCCGGCCATTCAA CAG in exon 14 (FBgn0052423:14) and sequence AAAGGT, which spans exons 14 and 16 (FBgn0052423:16), to rule out isoforms RA, RB, RD, RF, RH, and RI. Thus, the clone represents either *shep–RE* or *shep–RG*, which are identical throughout the region amplified for cDNA cloning. These primers and a third primer 5′-CCTGCTGGTTAAGTTTGCCGATGGCG-3′ were used to sequence verify all of the cDNA coding sequence except the first 29 bp at the 5′ end. The pUAST construct was injected into embryos by BestGene (Chino Hills, CA) to obtain *UAS–shep–RE/RG* insertions on the second chromosome.

Splice-trap expression patterns

Each splice-trap line was crossed with *UAS–mCD8::GFP*, and the third-instar larvae were collected and examined under a compound epifluorescence microscope without dissection. Larvae with CNS expression were dissected in Ca^{2+}-free saline solution [182 mM KCl, 46 mM NaCl, 2.3 mM $MgCl_2$•$6H_2O$, 10 mM 2-amino-2-(hydroxymethyl) propane-1, 3-diol (Tris), pH 7.2] and processed for immunostaining.

Antibody Generation

A 117 amino acid region of SHEP, common to all isoforms of the protein and showing no significant similarity to any other protein in the *D. melanogaster* genome, was chosen for antibody generation. This region is C-terminal to the two RNA Recognition Motifs (RRM-MSSPs) of SHEP, and begins at residue 447 after the ATG start site in SHEP protein isoform PA (see Flybase http://flybase.org). Primers that add an upstream *Eco*RI site (5′-ATCGAATTCCAGGTGGGTGGCTATCCAGTG-3′) and a downstream *Xho*I site (5′-TGACTCGAGTGATGCAGCT GTGCTAGCCTGTT-3′) were used to generate the required PCR fragment from *shep* cDNA clone LD29922 (Berkeley Drosophila Genome Project). After initial cloning into pCR4-TOPO (Invitrogen), the coding region was transferred to expression vector pGEX-6P-1 as an *Eco*RI/*Xho*I fragment to generate a GST-*shep* fused coding sequence. After induction, fusion protein was collected on a glutathione column. The SHEP region was released by cleavage with PreScission Protease (GE Life Sciences) and used to raise antibodies in a rabbit (Cocalico Biologicals, Inc).

Immunostaining

Immunostaining was performed as previously described (Hewes *et al.* 2003). After dissection in Ca^{2+}-free saline, tissues were fixed for 1 hr in 4% paraformaldehyde (PFA), 4% paraformaldehyde with 7% picric acid (PFA/PA), or

Bouin's fixative. We used antibodies against the following proteins: Bursicon α-subunit (1:5000, PFA/PA) (Luan *et al.* 2006), PHM (1:750, Bouin's) (Jiang *et al.* 2000), LK (1:500, PFA/PA), ILP2 (1:50, PFA/PA), Furin 1 (1:1000, Bouin's), RFamide (PT2 antiserum) (1:2000, PFA/PA), SHEP (1:1000, PFA/PA), choline acetyltransferase (1:100, PFA) (Developmental Studies Hybridoma Bank, DSHB, Iowa City, IA), Synapsin (1:20, PFA) (DSHB), Bruchpilot (1:20, PFA) (DSHB), and green fluorescent protein (GFP) (1:500, PFA) (Invitrogen, Carlsbad, CA). Secondary antibodies conjugated with Cy3 or ALEXA 488 from goat, mouse, and rat were each used at a 1:500 dilution. After incubation for 30 min in 70% glycerol, tissues were mounted in Vectashield (Vector Labs, Burlingame, CA), and confocal z-series projections were obtained with an Olympus (Center Valley, PA) Fluoview FV500 confocal microscope. For the isolated adult CNS images in Figure 4, we mounted the tissues between two cover slips and imaged from both sides; one of each pair of images was flipped horizontally and merged with the image from the other side in Adobe Photoshop (San Jose, CA) for better resolution of deep structures.

Immunostaining quantification

Cells and projections were imaged as confocal z-series scans, and identical settings were used in parallel for all of the samples in each experiment. Neuropil and soma areas were measured with Adobe Photoshop by manually tracing the structures and counting the bordered pixels on 2D maximum intensity projection images. For the larval stage, we measured the area of the more intensely immunostained bursicon neuron on the left side of abdominal segments 1–6 (A1–A6)—these cells survive through metamorphosis into the adult stage (Zhao *et al.* 2008). When the cells could not be clearly distinguished from each other (*e.g.*, due to close apposition), we substituted the cell from the right side in the same segment. The soma area for all six cells was then averaged to obtain a single value for each preparation. For the pharate adult stage, we measured the average soma area of the six most anterior bursicon neurons in the abdominal ganglia; preparations in which these six neurons could not be clearly delineated in the images (*e.g.*, due to physical juxtaposition of the cells) were discarded. Axonal branches of the bursicon cells were counted in Adobe Illustrator by Sholl analysis (Milosevic and Ristanovic 2007) after overlaying a grid of nested, concentric circles, each with a radius 50 μm larger than the previous circle, over the image. To measure the size of boutons within the axon projections of pharate adult bursicon neurons, we obtained confocal images (2D projections of z-series stacks) of the first left branch of the bursicon neuron axons within the abdominal nerve from the second abdominal segment (Ab_2Nv) (Demerec 1994). To ensure imaging of any more faintly immunostained boutons, the photomultiplier voltage was set to a level at which the centers of some boutons were saturated. We used the inversion and threshold functions in Adobe Photoshop (with the same threshold of 170 for all images) to convert the background to white and all remaining pixels, which were the boutons, to black. Boutons located within 50 μm distal and proximal of the first left branch in the Ab_2Nv were traced manually in Photoshop to obtain a count of the number of pixels, or cross-sectional area, for each bouton. For the quantification of wandering third-instar larval bouton areas, we applied a similar strategy for the bursicon cell neuromuscular junctions (NMJs) on muscles 12–13 of the second abdominal segment.

In situ hybridization

We used sense probe primer 5′-CGCGAATTCGCTTTGCC CGCATGGAGAGT-3′ and anti-sense primer 5′-GCGTCTA GAACCTGAGTCATCATGTAACCCGGAAT-3′ to demonstrate the expression pattern of *shep*. Single-strand DNA probes were amplified and labeled with digoxigenin by PCR, and *in situ* hybridization was conducted with probes at a 1:100 dilution using a previously described protocol (Hewes *et al.* 2003). For *in situ* hybridization on embryos, collections of embryos were made from apple juice-agarose plates every 24 hr.

Longevity assays under fed and starved conditions

For fed condition treatments, six vials each containing 10 3- to 5-day-old mated female flies were maintained at 25° and flipped to fresh food every day. The number of dead flies in each vial was scored every morning. For the starved condition, three to six vials of 10 1- to 2-day-old mated female flies of each genotype were maintained at 25° in vials with 1% agarose, which supplied water but no nutrients. Flies were scored every 3–4 hr from 8:00 AM to midnight, and the morning 8:00 AM count represented an 8-hr collection.

Flipping behavior assays

Larvae were placed on their backs on a piece of tissue that was soaked with 200 μl of phosphate buffered saline (PBS, 137 mM NaCl, 2.7 mM KCl, 10 mM Na_2HPO_4, and 1.8 mM KH_2PO_4) and set upon an apple juice-agarose plate, and the time required for each larva to right itself (so that the ventral surface was in contact with the tissue) was measured. Five measurements were obtained for each larva. For adults, the wings were removed and flies were allowed 2 hr to recover from the CO_2 anesthesia. Flies were placed individually in a 10-cm petri dish, which was tapped to flip each fly onto its back, and then the time for the fly to right itself was measured. Three trials were performed to obtain an average value for that fly; the *n* for each experiment indicates the number of animals tested.

Larval crawling behavior assay

We divided 100-mm plastic petri dishes evenly (by radius) into four concentric zones, numbered 1–4 from the center to the periphery. Dishes were filled with apple juice agarose,

and a thin layer of 200-μl PBS buffer solution was applied to the surface immediate prior to the assay. Each larva was placed into the center of zone 1 (center of the dish), and we recorded the total time the larva spent in each zone over a 10-min period.

Locomotor activity assays

Larval locomotor activity was scored on apple juice-agarose plates with a thin layer of PBS (200 μl) on the surface. Larvae were placed in the center of the plate and were allowed 2 min to acclimate. After that, we immediately began tracing the trail of the larva on the petri dish lid (viewed from directly above the plate) for 5 min. The trail of each larva was then placed on a square grid pattern (the side of each square was 6.35 mm), and we counted the number of squares traversed, counting squares more than once if the larva doubled back over a previous area. For the adult stage, flies were individually placed in an empty plastic vial that was vertically marked at 1-cm intervals. Flies were allowed to climb along the vial wall, and the maximum height attained in 5 sec was recorded. If flies fell off the side of the vial during the trial, the highest point attained was counted (rounding to the closest centimeter mark). If flies started climbing but failed to reach the first 1-cm mark, their maximum height attained was scored as 1 cm. Flies that did not climb during the test (~10% of the experimental group and none of the controls) were discarded.

Phylogenetic and sequence analysis

BLASTP searches with SHEP isoform PE were performed at NCBI (Altschul *et al.* 1997; Altschul *et al.* 2005) and Flybase (http://flybase.org/blast/) to obtain the top annotated vertebrate matches (domain similarity ≥50%, nonredundant, precalculated data version: cdd.v. 3.10, database: cdsearch/cdd, *E*-value threshold 0.01) and single representatives of each of the top three *Drosophila* protein family hits, respectively. The RNA recognition motif sequences of SHEP isoform PE, the vertebrate BLASTP matches, the *Drosophila* BLASTP matches and their vertebrate homologs, and two *Drosophila* outgroup RNA-binding proteins were aligned and used to build a neighbor-joining phylogenetic tree in MEGA5 (Tamura *et al.* 2011). Total percentage identity was calculated with LALIGN (Huang and Miller 1991), and the percentage identity for specific motifs was calculated using the NCBI BLASTP server. The sequence accession numbers for the proteins in the analysis were as follows: hMSSP-2, human MSSP-2 (*c-myc* single-strand binding protein 2) (NM002898); xMSSP-2, *Xenopus laevis* MSSP-2 (NM001086938); heMSSP-2, *Heterocephalus glaber* MSSP-2 (EHB06530); rMSSP-2, *Rattus norvegicus* MSSP-2 (NP001020574); mMSSP-2a, *Mus musculus* MSSP-2a (NP062685); zELAV-like 2, *Danio rerio* ELAV-like protein 2 (NM001002172); hRBP-PH, human RBP-PH (AAA69698); RBP9-PH, *Drosophila melanogaster* RBP9-PH (FBpp0288676); FNE-PB, *D. melanogaster* FNE-PB (FBpp0112400); hELAV, human ELAV (NP001410).

Mating behavior assay

All male and female flies for mating behavior assays were collected as isolated pharate adult pupae and were tested 3–5 days after eclosion. *Oregon R* was used as the wild-type control. Video recordings were obtained with a Sony DCR-SX45 camcorder, and they were stopped 10 min after copulation was completed (the recording in Supporting Information, File S5 was obtained by using an iPhone 4 to capture the monitor screen display obtained with a Sony ExwaveHAD camera on an Olympus SZX12 microscope). Flies that failed to initiate copulation within 30 min were discarded. Copulation latency was measured as the time required for the pair of flies to begin copulation. Mount latency was the time it took for the male to climb onto the back of the female (with both of the male's prothoracic legs clasping the base of the female's wings) after copulation started. The kicking index was calculated as the fraction of time the female spent kicking the male with her metathoracic legs during copulation. Grooming index was defined as the fraction of time the female spent grooming during the 10 min recording window after copulation. Some of the experimental flies displayed an unusual three-leg grooming behavior in which they rubbed both of the metathoracic legs together with one of the mesothoracic legs. The three-leg grooming index was calculated as the fraction of time each female fly spent performing this behavior out of the total time spent grooming during the recording window.

Statistics

All statistical tests were performed in SPSS 20.0 (IBM, Armonk, NY). Tukey honest significant difference (HSD) was used for all ANOVA *post hoc* tests. Statistical significance was indicated as $*P < 0.05$, $**P < 0.01$, $***P < 0.001$.

Results

Screen for loci with peptidergic neuron expression

We conducted a screen of 545 splice-trap insertion strains to identify genes with expression that was enriched in or specific to peptidergic neurons. Each splice-trap strain contained a *P*-element insertion with a *Gal4*-encoding exon that may be joined through alternative splicing with exons from a native gene into which the *P*-element is inserted. *Gal4* is therefore expressed in a pattern driven by the native gene (Lukacsovich *et al.* 2001). We used these lines to drive expression of membrane-tagged GFP (*UAS–mCD8::GFP*) to identify 38 insertions with reporter gene expression in the CNS of third-instar larvae. Although this set yielded useful lines (below) and we therefore did not perform further screening, the number of insertions with CNS expression was unexpectedly low, given the large number of genes expressed in selected CNS cells (*cf.* Berger *et al.* 2012; Fontana and Crews 2012). Two factors may have contributed to this low recovery rate: our live larval screening method, in which weaker CNS expression may have

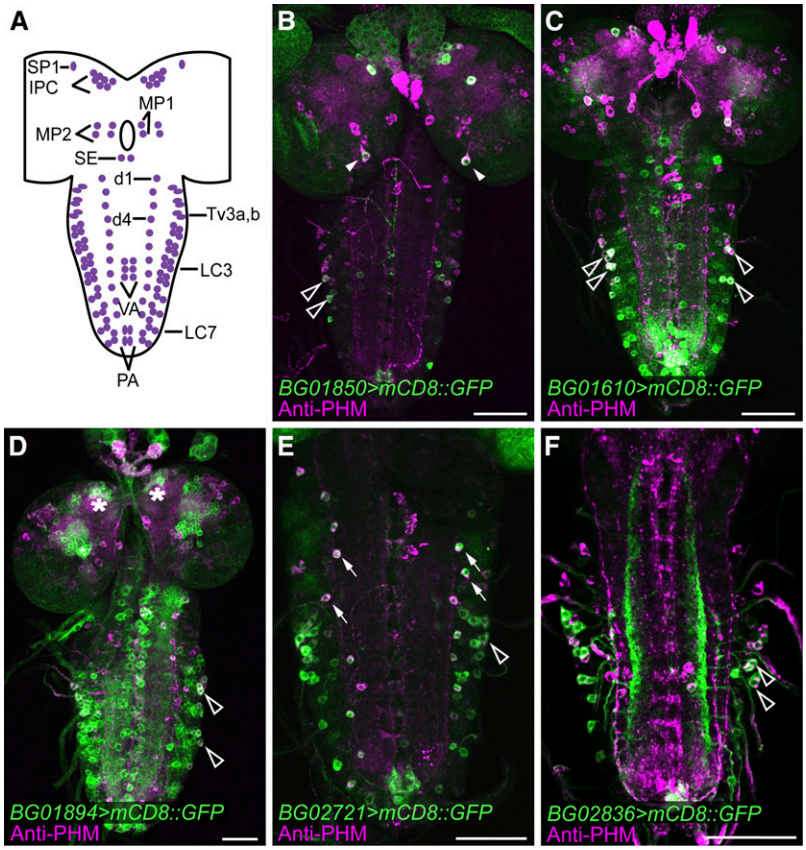

Figure 1 Colocalization of splice-trap reporter gene expression with the peptide biosynthetic enzyme, PHM. (A) Schematic of neurons that consistently display strong anti-PHM immunostaining in the wandering third-instar larval CNS. For cellular nomenclature, see Hewes *et al.* (2003). (B–F) Examples of reporter gene expression (green) and anti-PHM immunostaining (magenta) for five selected splice-trap insertions (*BG01850*, *BG01610*, *BG01894*, *BG02721*, and *BG02836*). Arrowheads, MP1 neurons; open arrowheads, LC neurons; asterisks, insulin-producing neurons (IPCs); arrows, dorsal chain neurons. Scale bars, 50 μm.

been missed, and the observation that 12–52% of splice-trap insertion sites with this vector (the rates co-vary with eye color) result in no detectable Gal4 activity (Lukacsovich *et al.* 2001).

Thirty of these insertions drove expression in neurons (Figure S1), and these were retained for further analysis. The other eight insertions drove expression in putative glia, ring gland cells, and/or neurites of undefined origin (data not shown) and were discarded. To identify insertions with expression in peptidergic neurons, we performed immunostaining for PHM in the 30 lines with expression of mCD8::GFP in CNS neurons. The PHM enzyme is required for amidation of most insect neuropeptides (Jiang *et al.* 2000) and is thus a global marker for peptidergic neurons (Hewes *et al.* 2003). We observed prominent PHM staining in 126 CNS neurons that could be reliably identified based on size, shape, and location (Figure 1A), and the insertion-driven expression patterns that included any of these cells were documented. Of the original 30 insertions with CNS reporter gene expression, 28 drove expression in different groups of PHM neurons, which included but were not limited to the brain insulin-producing cells (IPCs), medial protocerebrum neuron 2 (MP2), superior protocerebrum neuron 1 (SP1), medial protocerebrum neuron 1 (MP1), lateral cluster neurons (LC), adipokinetic hormone neurons (AKH) (Lee and Park 2004), dorsal chain neurons 1–11 (d1–d11), and posterior abdominal neurons (PA) (Hewes *et al.* 2003; Lee and Park 2004). Some of the insertions drove largely peptidergic cell-specific expression that was restricted to small cell groups (Figure 1, B and E, and Figure 2A), and some drove broader expression that included many other types of neurons (Figure 1, C and D).

To further characterize the peptidergic neurons included in each pattern, we double labeled the 28 lines that displayed peptidergic neuron mCD8::GFP expression with immunostaining for different neuropeptides that included CCAP, bursicon (BURS), ILP2, peptides with -RFamide C-terminal sequences, and LK, as well as the neuropeptide biosynthetic enzyme, Furin 1. We documented 17 insertions that drove expression in CCAP neurons, 8 with expression in ILP2 neurons, and 2–6 lines with expression in LK neurons, Furin 1 neurons, -RFamide neurons, and/or bursicon neurons (Figure S2, Figure S3, Figure S4, and Table 1).

Based on the genomic insertion sites, we were able to putatively identify the trapped gene for each of the 28 insertions (Table 1). When homozygous, 4 of the 28 insertions produced defects in ecdysis, post-ecdysis behaviors, and cuticular tanning, all of which are processes that are regulated by neuropeptides (Hewes *et al.* 2000; Park *et al.* 2002, 2003). Other mutant phenotypes included reduced adult tanning, appearance of multiple mouthparts in larvae, an ectopic wing vein, and wing expansion defects (Figure S5, A–D, and Table 1). Given the expression patterns and mutant phenotypes produced by these insertions, we deemed it likely that some of the trapped genes

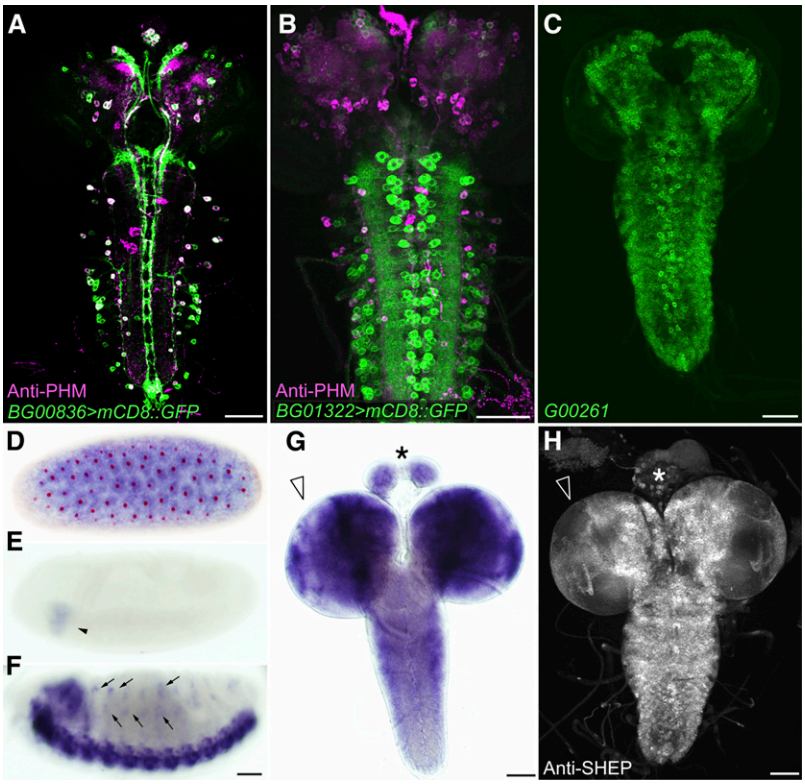

Figure 2 *shep* mRNA and SHEP protein expression in embryonic and larval stages. (A) $shep^{BG00836}$ displayed an mCD8::GFP reporter gene expression pattern (green) that overlapped extensively with anti-PHM immunostaining (magenta). The areas with the strongest colocalization appear white, but many other cells were labeled with both markers. (B) A second splice-trap insertion in the *shep* gene, $shep^{BG01322}$, showed a broader expression pattern, which included PHM-positive neurons as well as many PHM-negative neurons. (C) The protein-trap insertion, $shep^{G00261}$, also labeled a very broad population of neurons throughout the CNS. (D) In the embryonic syncytial blastoderm stage, *shep in situ* hybridization (purple) showed *shep* transcripts that were clustered around DAPI-labeled nuclei (red). The grayscale DAPI fluorescence image was inverted, with the black pixels (nuclear staining) converted to red, prior to the merge with the *in situ* image. (E) Zygotic transcripts of *shep* first appeared in the procephalic neurogenic region (arrowhead) in stage 7. (F) In late embryonic stages, *shep* transcripts were broadly detected throughout the CNS and PNS (arrows) by *in situ* hybridization. (G and H) In wandering third-instar larvae, *shep* transcripts and SHEP protein were broadly detected in the CNS and ring gland (asterisks) by *in situ* hybridization (G) and immunostaining (H), respectively. The distributions of *shep* transcripts and SHEP protein were not uniform, and we observed heterogeneous levels of expression in the brain lobes and ventral nerve cord, with lower level expression in the optic lobes (open arrowheads). Scale bars, 50 μm.

regulate the development or function of selected peptidergic neurons.

shep is expressed in a broad CNS pattern

One insertion, *BG00836*, had a reporter gene expression pattern that closely matched the cellular distribution of PHM (Figure 2A). At least three factors with similar expression patterns are known—DIMM, PHM, and PC2/amontillado—and all are key regulators of neuropeptide expression and/or peptidergic neuron development (Siekhaus and Fuller 1999; Hewes *et al.* 2003; Jiang *et al.* 2000). The peptidergic neurons contained within the *BG00836* expression pattern included neurons expressing ILP2, LK (Table 1), Furin 1, -RFamide (Figure S3), and bursicon (Figure S4). In addition, homozygous *BG00836* animals displayed defects in eclosion and wing expansion (Table 1), two behaviors under regulation by peptidergic neurons (Park *et al.* 2003; Peabody *et al.* 2008). Since *BG00836* contained a *P*-element insertion in an exon of *alan shepard (shep)* (Figure 3A), these behavioral defects, together with the high degree of colocalization between the *BG00836* ($shep^{BG00836}$) expression pattern and peptidergic markers, suggested a key role of *shep* in development or function of peptidergic neurons.

We obtained two other *P*-element insertions, $shep^{BG01322}$ and $shep^{G00261}$, in *shep* introns (Figure 3A). The $shep^{BG01322}$ insertion is a second splice-trap insertion in *shep* that we obtained in the initial screen (Figure S1), and it displayed widespread, low-level expression in the CNS (Figure 2B) together with higher-level expression in diverse peptidergic neurons (Figure S2, Figure S3, and data not shown). The $shep^{G00261}$ insertion is a protein-trap element, which attaches a GFP tag to the native protein (Morin *et al.* 2001), and this line displayed an even broader, more uniform pattern of CNS expression (Figure 2C). Thus, the SHEP expression pattern appeared to be broader than indicated by $shep^{BG00836}$, although two of the three lines displayed selected or stronger expression in some peptidergic neurons.

We employed *shep in situ* hybridization to confirm the *shep* mRNA expression pattern. To verify the specificity of the *in situ* probes, we first conducted hybridization with antisense probes to *shep* in *engrailed–Gal4/UAS-shep* (*engrailed>shep*) embryos, and we found the expected *engrailed* stripes (Figure S6A) in stage 11 embryos (Fox *et al.* 2010); *engrailed* stripes were not observed in wild-type embryos (Figure 2). This result confirmed both the function of the *UAS–shep* construct and hybridization of the antisense probe to *shep* transcripts. Sense probes were used as a control (Figure S6X).

In wild-type animals, we first observed hybridization to *shep* transcripts in oocytes, suggesting that *shep* is maternally loaded (Figure S6C). In syncytial blastoderm embryos at stage 3, *shep* transcripts were detected ubiquitously in a granular pattern surrounding nuclei (Figure 2D and Figure S6E). The level of *shep* transcripts decreased sharply in stage 4 embryos (Figure S6, G and H) and became undetectable by stage 5 (Figure S6I and

Table 1 Insertion sites, trapped genes, colocalized neuropeptide markers, and mutant phenotypes for insertions obtained through the splice-trap screen

Transposon insertion	Trapped gene(s)	Insertion site	Product(s) of trapped gene(s)	Colocalized neuropeptide markers	Homozygous mutant phenotype
BG00076	*Shal K+ channel interacting protein (SKIP)*	First exon	Ion channel regulating protein	DILP2, PHM, -RFamide	Recessive pharate adult lethality
BG00197	*jim*	537 bp upstream	Transcription factor	PHM	Midpupal lethality
BG00476	*CG4860*	4 bp upstream; insertion orientation unknown	Short-chain acyl-CoA dehydrogenase (SCAD)	PHM	Normal
BG00665	*CG8963*	Second intron of RA, RC and RD; first intron of RB	Poly(A) binding protein, middle domain of factor 4G (MIF4G) superfamily	CCAP, PHM	Larval lethality (all stages)
BG00836	*Alan shepard (shep)*	First exon of RC, RE (third intron of RB and RA, second intron of RD, and fourth intron of RF)	RNA-binding protein	CCAP, DILP2, DIMM, Furin 1, LK, PHM, -RFamide	20% pharate adult lethality; 2% adults failed to fully eclose and died stuck half-way out of the pupal case; 10% adults with wing expansion defects; 40% adults with ectopic longitudinal vein that extended from the posterior cross vein (pcv) (Figure S5)
BG01322	*Alan shepard (shep)*	15 bp upstream of RB; 1st intron of RD; second intron of RA and RF	RNA-binding protein	CCAP, DILP2 Furin 1, LK, PHM, -RFamide	25% adults with wing expansion defects
BG00855	*Homeodomain interacting protein kinase (hipk)*	First intron of RA and RB	Serine/threonine kinase	CCAP, PHM	Lethal
BG02654	*Homeodomain interacting protein kinase (hipk)*	First intron of RB	Serine/threonine kinase	CCAP, PHM	Normal
BG01140	*MYPT-75D*	Second intron of RA, RB and RD	Myosin phosphatase regulator	PHM	Normal
BG01171	*Adult enhancer factor 1 (Aef1)*	First exon of RB; first intron of RA, RC and RD	Transcription factor (C2H2 Zn finger)	CCAP, PHM	Moderate pupal lethality
BG01610	*scribbler (sbb)*	Second intron of RD, RE, RF and RJ; third intron of RG; insertion orientation unknown	Transcription factor	CCAP, PHM	Embryonic lethality
BG01711	*frizzled 2 (fz2)*	Fourth intron of RE and fifth intron of RD	Wnt receptor	CCAP, DILP2, PHM, -RFamide	Normal
BG01746	*taiman (tai)*	Second intron of RD and RG; third intron of RC, RE and RF	PAS domain transcriptional coactivator, signal transduction	CCAP, PHM	Moderate larval lethality associated with appearance of multiple mouthparts; moderate pupal lethality; adult dorsal thorax with darkened trident and less glossy cuticle
BG01766	*Decapping protein 2 (Dcp2)*	First exon of RA and RE; second intron of RB	mRNA decapping enzyme 2 (Dcp2p)	PHM	Early, mid-, and late pupal lethality
BG01850	*hephaestus (heph)*	First intron in RB	RNA recognition motif (RRM), RNA-binding protein	CCAP, DILP2, LK, PHM, -RFamide	Normal
BG01854	*ERp60*	First intron	Protein disulfide isomerase	PHM	Normal

(continued)

Table 1, *continued*

Transposon insertion	Trapped gene(s)	Insertion site	Product(s) of trapped gene(s)	Colocalized neuropeptide markers	Homozygous mutant phenotype
BG01894[a]	*CG11444*	First exon	Casein kinase substrate, phosphoprotein PP28 superfamily,	CCAP, PHM	Dark cuticle and trident on adult dorsal thorax
	CG32773	Second intron	Unknown		
BG02142	*cAMP-dependent protein kinase 1 (Pka-C1)*	First exon of RB and RC	Serine/threonine kinase	PHM	Midpupal lethality
BG02222	*CG30127*	Second intron	Unknown	CCAP, DILP2 PHM	Mid- to late-pupal lethality
BG02427	*CG42669*	First exon of RR, RU, RS and RQ; second intron of RE, RF, RL and RN; 1st intron of RM	Unknown	CCAP, PHM	Normal
BG02721	*Brain tumor (brat)*	First intron of RA and RD	Zn finger, B-box protein, translation repressor	CCAP, DILP2, LK, PHM	Normal
BG02759	*Protein kinase 61C (Pk61C, PDK1)*	First intron of RI; second intron of RD	Serine/threonine kinase	CCAP, PHM	Normal
BG02772	*CG13791*	First intron of RA and RB	BTB/POZ protein	CCAP, PHM	Normal
GT-000078	*CG13791*	First intron of RA; second exon of RB	BTB/POZ protein	CCAP, PHM	Normal
BG02810	*Couch potato (cpo)*	Second intron of RR, RT, RQ, RU, RW and RV	RNA recognition motif (RRM), RNA-binding protein	PHM	Lethality in homozygotes
BG02820[a]	*Chiffon (chif)*	First intron of RA and RB	Zn finger/DBF-like protein (ZnF-DBF)	PHM	Normal
	CG42231	First intron of RA	Unknown		
BG02836[a]	*6-Phosphofructo-2-kinase (Pfrx)*	First exon of RB and RG; first intron of RA, RF, RI and RJ;	6-phosphofructo-2- kinase (6PF2K)	DILP2, DIMM, LK, PHM, -RFamide	Normal
	CG14200	First intron of RA	Zinc finger/C2H2-like protein		
BG00449	*CG31145*	Second intron of RA, RB, RC and RD	Unknown	PHM	Mid- to late-pupal lethality

For insertions within exons or introns, the distances are provided with respect to the 5′ end of the exon or intron. For insertions upstream or downstream of the gene, the distances are relative to the transcriptional start or transcriptional stop site, respectively.

[a] Inserted in two overlapping or nested genes.

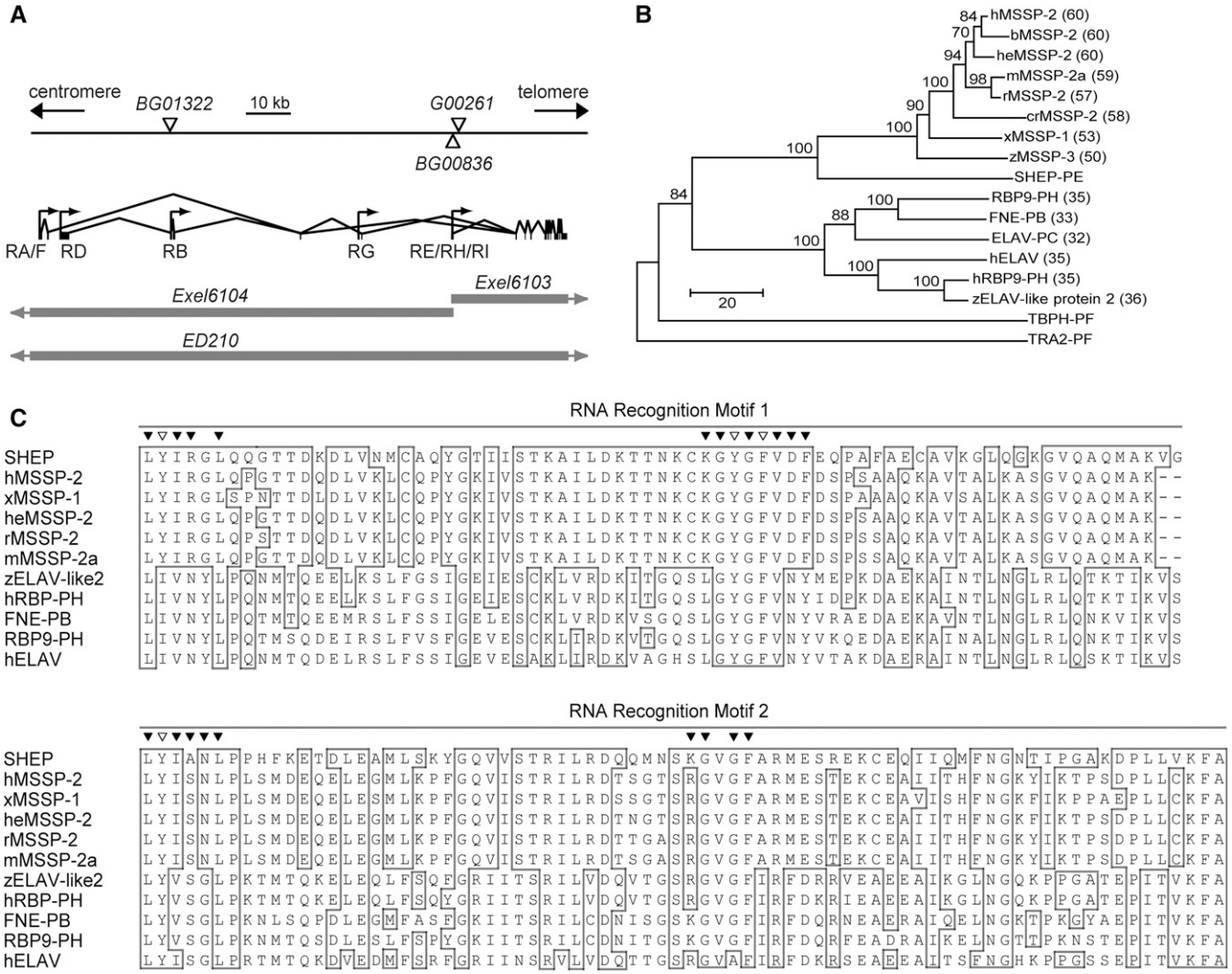

Figure 3 SHEP is the *Drosophila* ortholog to MSSP. (A) Genomic organization of alternative *shep* transcripts, *P*-element insertion sites, and regions deleted by deficiencies. Open triangles indicate the locations of *P*-element insertions, and the shaded bars indicate regions deleted by deficiencies (with shaded arrows indicating that the deficiency deletes flanking regions that are not shown in the figure). RA, RB, and RD–RI are *shep* transcripts arising from a combination of alternative transcriptional start sites (arrows) and alternative mRNA splicing. Vertical lines and bars represent exons, and the lines connecting them indicate introns. (B) A rooted neighbor-joining phylogeny tree for the SHEP–PE/G protein. Accession numbers for sequences in the tree are listed in the *Materials and Methods*. SHEP belongs to the MSSP family, and human MSSP-2 was the closest vertebrate homolog (shortest horizontal distance). The ELAV family was the next most closely related group, and TAR DNA-binding protein-43 homolog (TBPH) and Transformer 2 (TRA2) were more distantly related. Percentage identities obtained by BLASTP (NCBI) with SHEP–PE/G are shown in parentheses, and bootstrap scores for 100 cycles are indicated on the tree branches. (C) Alignment of RRMs of SHEP–E/G to 10 of the most closely related genes from the MSSP and ELAV families. Identical residues were highlighted in boxes and the most highly conserved residues found more generally in diverse proteins containing *ribonucleo*protein domains 1 and 2 (RNP1 and RNP2) (Bandziulis *et al.* 1989; Maris *et al.* 2005) were labeled with triangles across the top of the alignment. Among these most highly conserved residues, aromatic amino acids that form the primary RNA-binding surface in each RNP (Lorković 2012) were labeled with open triangles.

Figure S6J). At stage 7, zygotic *shep* expression first appeared in the procephalic neurogenic region (Figure 2E and Figure S6, K and L). The expression of *shep* transcripts was strongly upregulated in stage 8 and stage 9 (Figure S6, M–P) and expanded to a midline region, putatively mesectoderm, beginning in stage 10 (Figure S6Q and Figure S6R, arrows). Strong expression in the ventral neurogenic region started during stage 12 (Figure S6, S and T, open arrowheads) and spread to the entire CNS as well as to the peripheral nervous system (PNS) in stage 13 (Figure 2F arrows, and Figure S6, U and V, arrowheads). A developmental RNA-Seq expression profile from modENCODE (Graveley *et al.* 2011) largely mirrors the above results, with moderate expression in 0- to 2-hr embryos, a sharp drop in expression in 2- to 4-hr embryos, and a jump in expression in 12- to 14-hr embryos, when *shep* expression in our *in situ* analysis became strong and widespread throughout the CNS.

To determine the SHEP protein expression pattern, we performed immunostaining with a polyclonal anti-SHEP antiserum generated against a unique region common to all SHEP isoforms. We confirmed the specificity of the antiserum in *engrailed* > *shep* embryos, and the expected stripes were observed

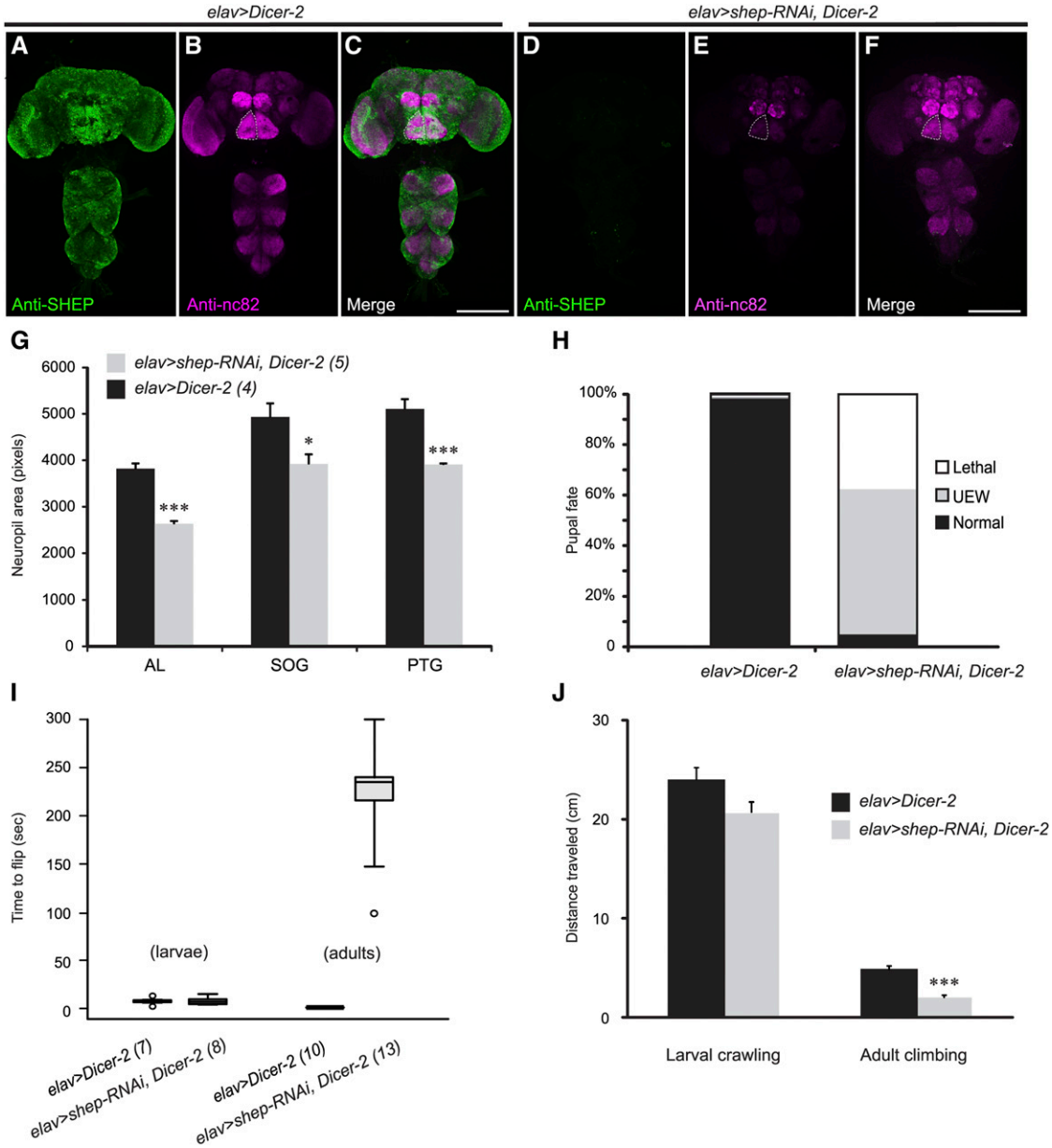

Figure 4 Developmental and behavioral defects following pan-neuronal *shep* RNAi. (A) Anti-SHEP immunostaining (green) revealed broad expression in the CNS of *elav* > *Dicer-2* control flies. (B) Immunostaining with anti-nc82 antibodies (magenta) showed the morphology of neuropils in *elav* > *Dicer-2* CNS. (C) In a merge of the images in A and B, strong colocalization of the two signals appears white. (D-E) *elav* > *shep–RNAi*, *Dicer-2* flies displayed marked reductions in anti-SHEP (D, green) and anti-nc82 (E, magenta) immunostaining. Neuropil areas were also reduced by 21–31%. Dashed outlines, left suboesophageal neuropil. Scale bars, 200 μm. (F) Merge of the images in D and E after enhancement (using a linear levels function in Photoshop) of the anti-nc82 signal for better visualization of neuropil outlines. (G) Quantification of selected neuropil areas from 2D projections of confocal z-series images. AL, antennal lobe; SOG, suboesophageal ganglion; PTG, prothoracic ganglion. $P = 0.000022$, repeated measures ANOVA; Tukey HSD *post hoc* (*) $P < 0.05$, (***) $P < 0.001$. The number of animals for each genotype is indicated in parentheses. (H) The final pupal or adult fate of *elav* > *shep–RNAi*, *Dicer-2* ($n = 272$) pupae and *elav* > *Dicer-2* ($n = 243$) controls. Lethal, died as pupae; UEW, adults with unexpanded wings; normal, adults with expanded wings. (I) Box plots of the time needed for larvae and adults to flip over when placed on their backs. The boxes define the interquartile range and the whiskers define the minima and the maxima. Open dots indicate outliers. The number of animals in each group is indicated in parentheses. (J) Distances crawled by *elav* > *shep–RNAi*, *Dicer-2* and *elav* > *Dicer-2* larvae (horizontal distance in 5 min on apple juice-agarose plates, $n = 15$–16) and adults (vertical distance in 5 sec in empty culture vials, $n = 18$-21). (***) $P < 0.001$, Student's *t*-test.

in stage 12 (Figure S6B). In wild-type animals, SHEP was first detected in the cytoplasm of oocytes (Figure S6D), and in syncytial blastoderm embryos it showed a granule-like distribution around the nuclei (Figure S6F), as we observed in the *shep in situ* hybridization. We did not observe strong zygotic SHEP expression in embryos until stage 17, when SHEP was detected in the cytoplasm of CNS and PNS neurons (Figure S6W, arrows). In stage 17, we also observed SHEP expression in the antennomaxillary complex and labral sensory complex (Figure S6W, arrowhead). In third-

instar wandering larvae, strong staining was broadly detected in the brain, ventral nerve cord, and ring gland (Figure 2H). Moreover, the pattern mirrored the results of *shep in situ* hybridization at this stage (Figure 2G). This broad expression of SHEP in the CNS was also detected at the P14 (Bainbridge and Bownes 1981) pharate adult stage (Figure 4A) and was concentrated in neuronal cytoplasm (data not shown).

Lower level expression of *shep* mRNA and SHEP protein was sometimes detectable in many nonneuronal tissues (data not shown), and this has been indicated by Western blot and RNA–Seq analysis (Graveley *et al.* 2011; Matzat *et al.* 2012). Nevertheless, these spatiotemporal expression data indicated that zygotic *shep* mRNA and SHEP protein was primarily restricted to the nervous system beginning in the late-embryo and continuing into the late-larval and pharate adult stages.

SHEP is a member of the MSSP RNA-/DNA-binding protein family

To date, eight *shep* transcripts (RA, RB, and RD–RI) have been identified (Figure 3A) based on expressed sequence tags (ESTs) reported by the Berkeley *Drosophila* Genome Project (BDGP). There are 53 *shep* 5′ ESTs, and RE, RH, and RI together represent ~70% of the total. To determine which of the three transcripts is more abundant, we randomly selected six ESTs that have been mapped to the shared 5′ end of the three transcripts for amplification and sequencing (see *Materials and Methods*). Four of the six clones contained the RE-specific sequence CAACAG from exon 13, and the other two did not and were therefore RH or RI. Thus, we used an RE/RG cDNA sequence to create a *UAS–shep* line. (RG utilizes an alternate transcriptional start site; however, the RE sequence amplified for the cDNA is identical to RG.)

The predicted *shep* open reading frame encodes six proteins PA, PB/D, PE/G, PF, PH, and PI (the predicted protein products of transcripts RB and RD are identical, and the products of RE and RG are identical). These isoforms have diverse N termini and largely share the same C-terminal sequences, except for two short indels. All six predicted SHEP isoforms contain two RNA recognition motifs (RRM) (Figure 3C), suggesting possible binding to RNA. According to a protein-sequence-based neighbor-joining phylogenetic tree, SHEP–PE displayed the strongest homology with the MSSP (*c-myc* single-strand binding proteins) family, which consists of RNA-/DNA-binding proteins. The most closely related protein to SHEP in vertebrates was human MSSP-2, with a sequence identity of 60% for conserved feature regions (Figure 3B) (Marchler-Bauer *et al.* 2005) and 38% for the global alignment. After MSSP, the next most closely related protein(s) was a family of mRNA-binding/alternative splicing factors that includes *Drosophila* ELAV (Figure 3B).

Loss of neuronal shep resulted in developmental and behavioral defects

Since *shep* was primarily and broadly expressed in CNS, we obtained pan-neuronal *shep* loss-of-function animals by crossing *elav–Gal4* to *UAS–shep–RNAi*, *Dicer-2* (*elav* > *shep–RNAi*, *Dicer-2*) to assay impacts on the CNS. The efficiency of the *shep* RNAi was confirmed by anti-SHEP immunostaining on the CNS of *elav* > *shep–RNAi*, *Dicer-2* flies at the P14 pharate adult stage. The levels of SHEP protein were strongly reduced by *shep–RNAi*, *Dicer-2*, and only a few SHEP-positive neurons throughout the entire CNS were detected (Figure 4, A and D).

We used the presynaptic marker, Bruchpilot (monoclonal antibody nc82) (Seki *et al.* 2010), as a general counterstain for the above anti-SHEP immunostaining. Interestingly, the expression level of Bruchpilot was also decreased in pharate adults (Figure 4E) and third-instar larvae (Figure S7, A and B). Based on this finding, we examined two other presynaptic markers, choline acetyltransferase (ChAT) and synapsin, and both displayed substantially reduced expression throughout the CNS (Figure S7, C–F). These results suggest that *shep* RNAi led to smaller or fewer synapses, or reduced expression of multiple synaptic proteins. This was accompanied by a decrease in neuropil size. In spite of the weak anti-Bruchpilot signal in *elav* > *shep–RNAi*, *Dicer-2* flies, we were able to visualize neuropilar regions, and we found a 21–31% reduction of multiple neuropilar areas, including the antennal lobes, suboesophageal ganglion, and prothoracic ganglion (Figure 4G). Interestingly, we also observed substantial loss of mCD8::GFP reporter gene expression (suggesting failure to differentiate or cell loss) in adult wing sensory neurons following *shep* RNAi with a *D42–Gal4* driver (Figure S5, E–H).

About one-third (38%) of *elav* > *shep–RNAi*, *Dicer-2* flies died as pupae, while the lethality observed in *elav* > *Dicer-2* control flies was <1% (Figure 4H). Most (74%) of the *elav* > *shep–RNAi*, *Dicer-2* lethality occurred late during pupal development in animals that displayed wing pigmentation (stage P12 or later), and the rest of the lethality occurred during eclosion. These flies emerged halfway from the pupal case and then remained stuck there permanently. The half-eclosed phenotype may have been the result of weakened eclosion movements, since *elav* > *shep–RNAi*, *Dicer-2* flies that did eclose walked unsteadily and often fell to the bottom of the vial, and *elav* > *shep–RNAi*, *Dicer-2* flies during eclosion appeared to display weakened leg movements (data not shown). More than 92% of the escaper *elav* > *shep–RNAi*, *Dicer-2* adults also failed to expand their wings after eclosion (Figure 4H). The eclosion defects and wing expansion defects following *shep* RNAi were consistent with the phenotype observed for homozygous $shep^{BG00836}$ mutant animals (Table 1), indicating that these effects of the *shep* RNAi are due to loss of SHEP function rather than off-target effects of the RNAi.

In addition to the developmental or motor defects, we also observed reduced life span. In a life span experiment with flies maintained on standard food, all *elav* > *shep–RNAi*, *Dicer-2* adults died by the 18th day, while none of the *elav* > *Dicer-2* control flies died during this time period (Figure S8A). This result is consistent with previous reports of genetic screens, which showed that *shep* mutants might

have significantly higher fat accumulation in larvae (Reis *et al.* 2010), possibly reflecting a reduced mobilization of fat reserves, and reduced starvation tolerance in adults (Harbison *et al.* 2004). We observed similar defects in starvation tolerance in multiple *shep* loss-of-function backgrounds (Figure S8, B–D). Thus, reduced expression of *shep* in the nervous system resulted in weakened adult locomotor behaviors, failure to complete neuropeptide-controlled eclosion and wing expansion behaviors, and shortened life span under fed and starved conditions.

To quantify the effects of reduced *shep* expression on locomotor behaviors, we measured rates of flipping and climbing in two separate assays. In the flipping assay, we removed the wings of adult flies and then placed them on their backs. Although the *elav > shep–RNAi*, *Dicer-2* flies waved their legs around rapidly while flipped, they took >200 times longer to turn over than the control *elav > Dicer-2* flies (Figure 4I). We also performed flipping assays on $shep^{Exel6103}/shep^{Exel6104}$ mutant animals, and they took 10 times longer to flip over than the hemizygous deficiency control animals (data not shown). The $shep^{Exel6103}$ and $shep^{Exel6104}$ deficiencies share a common breakpoint located within the first exon shared by *shep* transcripts RE/RH/RI; $shep^{Exel6103}$ deletes all of the 3′ exons, which include the coding sequences for the C-terminal parts of the SHEP protein that are shared by the various SHEP isoforms, and $shep^{Exel6104}$ deletes all of the *shep* exons 5′ of the breakpoint, which include some coding sequences (Figure 3A). Western blot analysis showed that $shep^{Exel6103}/shep^{Exel6104}$ mutant animals lack expression of the SHEP–PA and –PB/D isoforms and have reduced expression of SHEP–PE/G (Matzat *et al.* 2012).

In the climbing assay, which measured the vertical distance traveled in 5 sec after each fly started climbing, *elav > shep–RNAi*, *Dicer-2* flies traveled only 42% of the vertical distance that was covered by the *elav > Dicer-2* control flies (Figure 4J). The reduced distance climbed appeared to result at least partially from motor defects or weakness, since we observed that the legs of the *elav > shep–RNAi*, *Dicer-2* flies shook while climbing and these flies often dropped off the side of the vial during the 5 sec period. Taken together, these general locomotor defects, the observed reductions in neuropil area (Figure 4G), the loss of adult wing sensory neurons (Figure S5), and the broad expression of SHEP in the CNS (Figure 4A) suggest that SHEP regulates the development or function of many motorneurons, interneurons, and/or sensory neurons.

Interestingly, the *shep* RNAi did not result in changes in flipping or crawling performance in third-instar larvae (Figure 4, I and J). Moreover, the third-instar larval neuropil area was also unchanged (Figure S7G), which was in contrast to the reduction in neuropil area that we observed at the P14 pharate adult stage (Figure 4, A–G). The stage dependence of these behavioral and morphological phenotypes suggested that *shep* might regulate nervous system development primarily during metamorphosis, when the nervous system undergoes dramatic structural remodeling. Consistent with this model, RNA–Seq analysis shows a strong peak of *shep* expression during the first half of metamorphosis, beginning in late third-instar wandering larvae (salivary gland puff stages 3–6) and continuing through 2 days after pupariation; levels then decline by ~50% during the third day after pupariation (Graveley *et al.* 2011).

It appeared that SHEP regulated cell growth in the above tests primarily during metamorphosis, but the effects were not exclusive to this stage, and we did detect a subtler behavioral defect in larvae, which displayed more turns and a tendency to remain in the center of the petri dish in the distance crawled assays (Figure S9). These results show that loss of SHEP function in the larval nervous system resulted in some behavioral defects. Nevertheless, the behavioral defects in larvae were qualitatively weaker overall than the ones observed in adults (Figure 4, I-J).

Loss of shep resulted in altered mating behaviors

In addition to the general locomotor defects seen in *shep* mutants, we observed changes in the organization of mating behaviors. We first detected this phenotype in $shep^{Exel6103}/shep^{Exel6104}$ females, which laid only unfertilized eggs when crossed to $shep^{Exel6103}/shep^{Exel6104}$ males but did produce viable embryos and larvae when crossed to wild-type (*Oregon R*) males. This result led us to examine courtship and mating behaviors in the $shep^{Exel6103}/shep^{Exel6104}$ adults. Virgin $shep^{Exel6103}/shep^{Exel6104}$ females displayed several sexual rejection behaviors. These included decamping, failure to extend the wings to allow copulation, kicking to push males off during copulation (Tan *et al.* 2013), and expulsion of seminal fluid after copulation.

We quantified these changes in $shep^{BG00836}/shep^{ED210}$ females, which also displayed these defects in courtship and mating behaviors. The $shep^{ED210}$ allele deletes the entire *shep* gene (Ryder *et al.* 2007), and $shep^{BG00836}$ carries a *Gal4* splice-trap element that is inserted in a *shep* exon (Figure 3A), and $shep^{BG00836}/shep^{ED210}$ females display reduced expression of native SHEP protein (Figure S10C) (Matzat *et al.* 2012). Wild-type males were paired together with wild-type females or $shep^{BG00836}/shep^{ED210}$ females with or without *shep* (*UAS-shep*) rescue. All three genotypes showed similar copulation latencies (Figure 5A). Once copulation started, wild-type virgin females extended their wings and allowed mounting of males within seconds (File S1), but $shep^{BG00836}/shep^{ED210}$ virgin females vigorously kicked at males while keeping their wings closed, thus preventing the males from mounting and grasping the base of the wings (Figure 5A and File S2). During copulation, the $shep^{BG00836}/shep^{ED210}$ females also kicked almost continuously (>90% of the time) at the males with their metathoracic legs, whereas the wild-type females displayed kicking behaviors only 17% of the time (Figure 5B). The copulation duration was reduced in the $shep^{BG00836}/shep^{ED210}$ females (Figure 5A), and we often observed a burst of intensive kicking prior to the withdrawal of the male (data not shown). Kicking during both mounting and copulation was reduced in

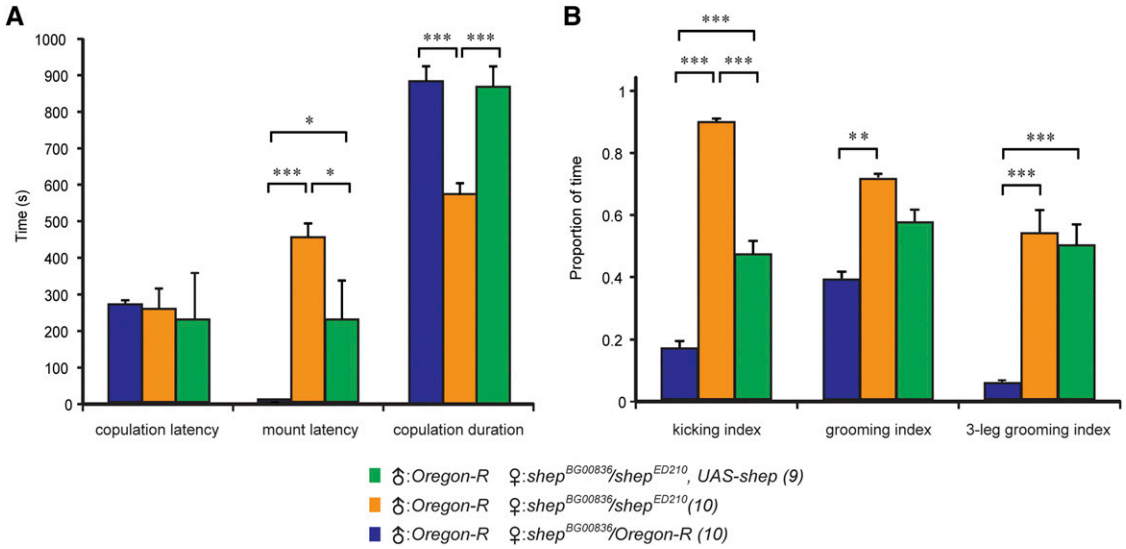

Figure 5 Virgin *shep* mutant females displayed increased rejection of courting males. (A) Virgin females of all genotypes displayed the same latency to copulation with *Oregon R* males, but the mount latency was increased and copulation duration was decreased for $shep^{BG00836}/shep^{ED210}$ mutant females. Rescue with *UAS–shep* returned these values to control levels. The numbers following the genotypes are the sample sizes. (B) Postcopulation behaviors for the females in A. All latency and duration data were measured in seconds (A), and each index is the ratio of the duration of a given behavior over the 10-min postcopulation video recording period. Separate one-way ANOVAs were performed for each behavioral measure (copulation latency, $P = 0.891$; mount latency, $P = 0.000015$; copulation duration, $P = 0.000234$; kicking index, $P = 0.000027$; grooming index, $P = 0.035767$; three-leg grooming index, $P = 0.000906$). (*) $P < 0.05$, (**) $P < 0.01$, (***) $P < 0.001$, Tukey HSD *post hoc* test.

$shep^{BG00836}/shep^{ED210}$, *UAS–shep* females, and the copulation duration was restored to the wild-type level (Figure 5, A and B).

After copulation, $shep^{BG00836}/shep^{ED210}$ females displayed extensive grooming, almost exclusively involving just the legs (Figure 5B, grooming index, and File S3). In contrast, control females used the metathoracic legs to alternate grooming of the legs, wings and abdomen (File S4). Much of the grooming in recently mated $shep^{BG00836}/shep^{ED210}$ females involved one of the mesothoracic legs together with the metathoracic legs (File S3); this form of three-leg grooming was rarely observed in wild-type flies (Figure 5B and File S4). In addition, we observed 8 of 10 females actively expelling seminal fluids from the reproductive tract (File S5); we never observed the expulsion of seminal fluids by wild-type females. Females often used their metathoracic legs in this process, and as shown in the video, strands of sticky fluid could be observed. Thus, the presence of these fluids may have contributed to the observed changes in grooming behavior. We did not observe rescue of normal rates of two-leg grooming in $shep^{BG00836}/shep^{ED210}$, *UAS–shep* females, although this failure to rescue was not completely unexpected, given the heterogeneous pattern of transgene expression (which may not include important grooming circuits) in the $shep^{BG00836}$ line (Figure 2A).

shep was required for neuronal outgrowth during metamorphic remodeling

Since we observed wing expansion defects in *shep* mutants, we examined the function of *shep* in the bursicon neurons, which play a key role in the regulation of wing expansion behaviors (Peabody *et al.* 2008). These neurons undergo extensive remodeling during metamorphosis and secrete the neuropeptide bursicon soon after eclosion to promote wing expansion behaviors (Peabody *et al.* 2008; Zhao *et al.* 2008). To test whether *shep* regulated the development or function of the bursicon neurons, we examined these cells in hemizygous $shep^{BG00836}/shep^{ED210}$ mutant animals. The cells were visualized by immunostaining with an anti-bursicon (bursicon α-subunit, FBgn0038901) antiserum (anti-BURS) (Luan *et al.* 2006) or by expressing the membrane tag, mCD8::GFP. Both markers provided excellent resolution of the bursicon neuron somata (Figure S4), and the peripheral axons and axon terminals in both larvae and P14 stage pharate adults in *shep* loss-of-function backgrounds (Figure S11). Thus, we used anti-BURS in most experiments, since this marker did not require the introduction of *UAS–mCD8::GFP* into all genotypes.

At the P14 pharate adult stage, the bursicon neuron somata in $shep^{BG00836}/shep^{ED210}$ animals lost the multiangular morphology that is characteristic of that stage (Figure 6A) and became more rounded (Figure 6B) together with a 27% reduction in soma area (Figure 6J). In $shep^{Exel6103}/shep^{Exel6104}$ animals, $shep^{BG00836}$ homozygotes, and *ccap > shep–RNAi* animals (the abdominal bursicon neurons are a subset of the CCAP neurons) (Luan *et al.* 2006), the soma area reductions were all 42–47% (Figure S10F). In the periphery, we also observed reduced branching of the bursicon neuron axons in P14 pharate adult stage animals (Figure 6, D and E), and we quantified the changes in branch numbers by Sholl analysis (Magarinos *et al.* 2006) (Figure 6K). We observed no difference between $shep^{BG00836}/shep^{ED210}$

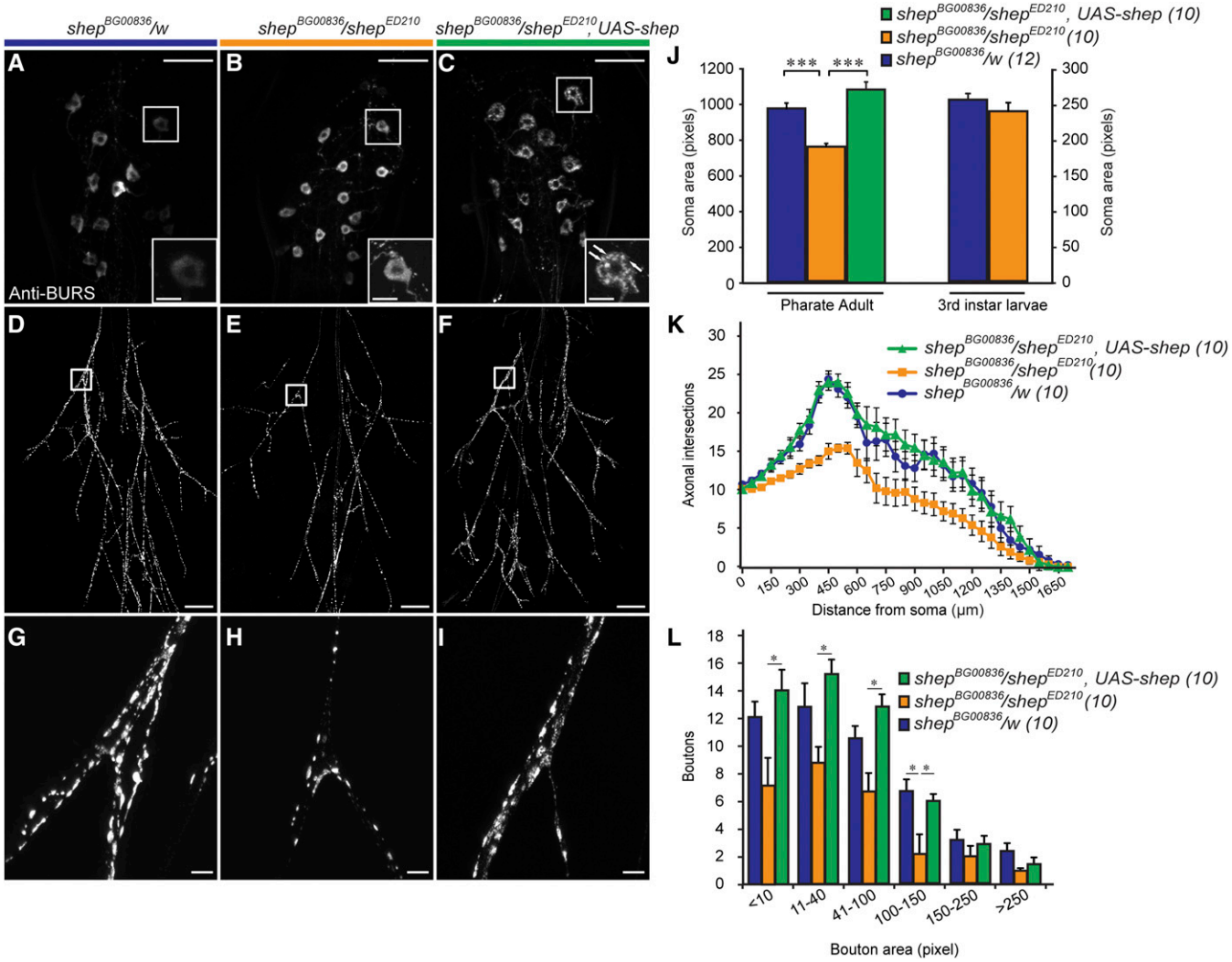

Figure 6 Loss of *shep* in *shep*^{BG00836}/*shep*^{ED210} animals reduced the soma area, branching of peripheral axons, and the bouton size distribution of bursicon neurons at the P14 pharate adult stage. (A–C) Immunostaining with anti-BURS antibodies showed the morphology of bursicon neurons in the abdominal ganglia. The most anterior cell on the right side is shown in the insets, with punctate peptide accumulation in the *shep*^{BG00836}/*shep*^{ED210}, *UAS–shep* cell labeled by arrows. (D–F) Reduced branching of the bursicon neuron axons in the peripheral arbor in a *shep*^{BG00836}/*shep*^{ED210} pharate adult (E) and rescue of branching in a *shep*^{BG00836}/*shep*^{ED210}, *UAS–shep* animal (F). (G–I) A reduction in bouton sizes in *shep* mutant animals (H) and rescue after targeted expression of *shep* (I) was also observed in the peripheral axon arbor. Scale bars, 50 μm (insets in A–C, 10 μm). (J) Quantification of bursicon neuron soma areas for P14 pharate adults and wandering third-instar larvae. We performed a one-way ANOVA ($P < 0.000001$, Tukey HSD *post hoc*, ***, $P < 0.001$) for the pharate adult values and a Student's *t*-test ($P = 0.934$) for the wandering third-instar larval values. (K) Results of Sholl analysis of branches in the peripheral axon arbor. The space between each of the concentric rings used to count intersecting axons was 50 μm. (L) Counts of boutons along all axons 50 μm proximal and distal to the first branch of the Ab_2Nv nerve (squares). (*) $P < 0.05$ (two-way ANOVA, $P < 0.00001$; Tukey HSD *post hoc* test. Scale bars, 100 μm.

animals and *shep*^{BG00836}/*w* controls in the number of efferent bursicon axons at the point where they enter the abdominal nerves or in the maximum extent of these axons in the periphery (Figure 6K). However, the axons in *shep*^{BG00836}/*shep*^{ED210} animals had fewer peripheral branches, resulting in fewer intersections with the intermediate sampling rings (Figure 6K). The reduction in intersections was evident throughout the arbor, and the greatest reduction (10 fewer branches) was observed 450 μm from the posterior tip of the ventral nerve cord. The peripheral bursicon axons in *shep*^{BG00836}/*shep*^{ED210} pupae also displayed fewer boutons than the controls (Figure 6, H and L). We observed similar defects in axonal branching in *shep*^{Exel6103}/*shep*^{Exel6104}, *ccap* > *shep–RNAi*, and *ccap* > *shep–RNAi*, *Dicer-2* animals (Figure S12, A–C). These peripheral axon branches form during outgrowth of the bursicon neurons during metamorphosis, after pruning of the larval, unbranched axons has occurred (Zhao *et al.* 2008). Taken together, these results show that *shep* promotes formation (or maintenance) of peripheral axon branches in the bursicon neurons during metamorphic remodeling.

To determine whether the cellular defects were caused solely by the loss of *shep*, we took advantage of the fact that the *shep*^{BG00836} mutation can be used to drive transgene

expression in *shep*-mutant bursicon neurons. In P14 stage $shep^{BG00836}/shep^{ED210}$, *UAS–shep* pharate adults, we found that bursicon neuron soma area, peripheral axon branch number, and bouton number were all fully rescued (Figure 6, C and F; I–L). Since we built *UAS–shep* with *shep–RE/RG*, we conclude that one or both of these isoforms are sufficient to restore normal soma growth, peripheral axon branching, and bouton growth in the bursicon neurons during metamorphic remodeling. In addition, we observed punctate accumulation of bursicon in the somata (cytoplasm) of *shep*-rescued neurons (Figure 6C), suggesting that *shep* expression can influence the regulated secretory pathway. However, we did not observe changes in bursicon distribution in *shep* mutant cells without rescue, and we therefore cannot exclude the possibility that this observation reflects a gain-of-function effect of transgenic SHEP expression in the $shep^{BG00836}/shep^{ED210}$, *UAS–shep* animals.

Interestingly, loss of *shep* had no impact in our assays of bursicon neuron morphology in wandering third-instar larvae. In contrast to pharate adults, bursicon neuron soma area was unchanged in $shep^{BG00836}/shep^{ED210}$ larvae (Figure 6J). Similarly, although $shep^{Exel6103}/shep^{Exel6104}$ and $shep^{BG00836}/shep^{BG00836}$ P14 pharate adults each displayed a 44–47% reduction in bursicon neuron soma area, these genotypes displayed no change in soma area in the third-instar larvae. In addition, there was no change in bursicon neuron soma area in *ccap > shep–RNAi*, *Dicer-2* larvae (Figure S10G). To test for impacts of the loss of *shep* on larval bouton area, we examined boutons at the bursicon neuron NMJ on muscles 12–13 of the second abdominal segment (Hodge *et al.* 2005). In $shep^{Exel6103}/shep^{Exel6104}$, $shep^{BG00836}/shep^{ED210}$, and *ccap > shep–RNAi*, *Dicer-2* larvae, we found no change in the number and size distribution of NMJ boutons (Figure S12, D–L), which is in contrast to the clear reductions in bouton area and number in P14 stage pharate adult $shep^{BG00836}/shep^{ED210}$ animals (Figure 6, G-H and L). Taken together, these results suggest that SHEP is required for growth of the bursicon neurons during metamorphosis but not during larval development.

Discussion

Identification of shep through splice-trap screening

Through an expression pattern-based splice-trap screen, we identified 28 insertions that drove expression in peptidergic neurons. These included 17 insertion sites with expression in CCAP neurons and several sites with expression in ILP2 neurons, LK neurons, Furin 1 neurons, -RFamide neurons, and/or bursicon neurons (2–8 sites per marker). One of the insertions, $shep^{BG00836}$, drove transgene expression in PHM-positive peptidergic neurons, and homozygous $shep^{BG00836}$ adults displayed defects in wing expansion. These observations implicated *shep* in the development or function of diverse peptidergic neurons, and we selected it for further analysis. Anti-SHEP immunostaining and additional *shep* reporter genes confirmed expression in peptidergic neurons, but these markers and *shep in situ* hybridization also revealed widespread expression in the CNS, with much lower expression in other tissues.

SHEP is orthologous to the c-myc single-strand binding protein, MSSP-2

Previous studies have described *shep* as homologous to the vertebrate genes, Rbms2/Scr3 (Armstrong *et al.* 2006) or Rbms1/Scr2/MSSP-2 (Wang *et al.* 2013). Our phylogenetic analysis supported the placement of SHEP in the MSSP family, with the ELAV family of RNA-binding proteins being the next most closely related (Figure 3B). In general, MSSP proteins contain RNA recognition motifs and have been found in vertebrates to bind DNA, RNA, or proteins to regulate a variety of biological processes, including DNA polymerization, gene expression, cell transformation, and apoptosis (Balducci-Silano *et al.* 1998; Kimura *et al.* 1998; Niki *et al.* 2000a,b; Nomura *et al.* 2005). In *Drosophila*, SHEP interacts with the insulator proteins Mod(mdg4)2.2 and Su(Hw) to negatively regulate chromosomal insulator activities, specifically in the CNS (Matzat *et al.* 2012). These molecular insights suggest a gene regulatory mechanism by which SHEP may control aspects of the metamorphic development of the bursicon neurons, as well as other neurons that contribute to the overall structure of adult brain neuropils.

Metamorphic remodeling of the bursicon neurons and stage dependence of SHEP function

The *shep* mutant defects in wing expansion presented an opportunity to define cellular functions of SHEP in an experimentally accessible cell type, the bursicon neurons. In *shep* mutants, we observed a reduction in the postpruning growth of the bursicon neurons during metamorphosis, resulting in smaller somata and less branching in the peripheral axon arbor in pharate adult animals (Figure 6).

Interestingly, the regulation of bursicon neuron growth by *shep* was stage dependent. We observed defects in bursicon neuron soma growth and axon branching during metamorphosis in hypomorphic *shep* mutant animals of multiple genotypes, including $shep^{BG00836}/shep^{BG00836}$, $shep^{Exel6103}/shep^{Exel6104}$, and $shep^{BG00836}/shep^{ED210}$ (Figure S10 and Figure S12). However, in each of these genotypes, the larval cellular morphologies were normal.

We observed other behavioral defects that suggested that the metamorphosis-specific actions of SHEP were not limited to the bursicon neurons. For example, the most severe *shep* loss-of-function genotype tested (see below) was *elav > shep–RNAi*, *Dicer*-2, but *elav > shep–RNAi*, *Dicer*-2 larvae displayed normal crawling distances and self-righting behaviors, while this genotype showed lethality in the late pupal stages and severe locomotor defects in adult animals. Associated with this increase during metamorphosis in the dependence of the nervous system on *shep* activity, the levels of *shep* expression increase markedly at the onset of metamorphosis (Graveley *et al.* 2011). These results provide indirect evidence to suggest that an increase in *shep* expression

during the pupal stage may support neuronal remodeling or other aspects of neuronal function and development in diverse neurons during metamorphosis.

Although most of the larval behaviors assayed were unaffected in *shep* mutant animals, we observed one behavioral phenotype in *elav > shep–RNAi*, *Dicer-2* larvae, namely a tendency to remain in the center of the apple juice-agarose plate while making many sharp turns along the path of locomotion. Based on anti-SHEP immunostaining (Figure S10, A–E), *UAS–shep–RNAi*, *Dicer-2* provided a more complete knockdown of anti-SHEP immunostaining in the CNS than *shep* RNAi without *UAS–Dicer-2* or in $shep^{BG00836}$ homozygotes or $shep^{BG00836}/shep^{ED210}$ mutant larvae. Moreover, *shep* RNAi without *UAS–Dicer-2* led to a greater knockdown of SHEP in Western blots than $shep^{Exel6103}/shep^{Exel6104}$ (Matzat *et al.* 2012). Taken together with the above observation that many of the weaker *shep* loss-of-function genotypes had defects that were only manifest in adults, these findings suggest that *shep* plays a stage-dependent (largely metamorphosis-specific) role in the maintenance, function, or development of the nervous system.

Broad impacts of shep in the nervous system

The SHEP expression pattern and *shep* mutant phenotypes reported here are consistent with broad actions of this protein in neuronal development and functions throughout the nervous system. Pan-neuronal loss of *shep* resulted in late-pupal lethality and reduced adult life span under both fed and starved conditions, as well as diverse developmental and behavioral defects, including failure to complete wing expansion, uncoordinated and weakened adult locomotion, reduced neuropil areas, and altered mating behaviors. Other groups have also shown defects in gravitaxis and reduced starvation resistance in *shep* mutants (Harbison *et al.* 2004; Armstrong *et al.* 2006).

Such widespread actions may also explain the partial rescue of the mating defects by *UAS–shep* expression in $shep^{BG00836}/shep^{ED210}$ females. Although we cannot exclude the possibility that other SHEP isoforms in addition to SHEP–E/G (used to create *UAS–shep*) were necessary to support the normal function of the postcopulatory grooming circuits, it is also possible that neurons required for female receptivity to the male may have been included in the $shep^{BG00836}$ expression pattern used to drive *shep* rescue, whereas the neurons involved in normal postcopulatory grooming behaviors were not.

The observation of several seemingly independent behavioral defects (*e.g.*, gravitaxis and female receptivity to mating) and reduced neuropil areas, taken together with the cellular defects described in *shep*-mutant bursicon neurons, suggests that SHEP may have pleiotropic effects on neurite development or other processes throughout the CNS. Such pleiotropic effects of *shep* mutations in the CNS may be due to the loss of SHEP suppression of widely distributed chromatin insulator complexes (Matzat *et al.* 2012), so as to establish altered chromatin states and gene expression, potentially in multiple signaling pathways controlling a range of developmental and physiological events. In addition, some of the adult *shep* loss-of-function phenotypes, such as reduced life span and altered mating behaviors, may reflect adult-specific (acute) effects of SHEP on neuronal activity. Alternatively, the metamorphosis-specific regulation of neurite branching and cell growth in the bursicon neurons may be representative of the actions of SHEP in many neuronal cell types. It will be important in future studies to distinguish among these models, as our results demonstrate that SHEP is a general regulator of the postembryonic development of mature neurons.

Acknowledgments

We thank Bruce Roe (University of Oklahoma) for the competent DH5α *E. coli*, Rebecca A. Simonette for expert assistance in preparation of the SHEP antibody, and Ingo Schlupp (University of Oklahoma) for statistical methods assistance. Montgomery Simms and George Malatinszky (University of Oklahoma) assisted with the behavioral assays. This work was supported by grants to R.S.H. from the National Science Foundation (IBN-0344018 and IOS-0744447) and to K.M.B. from NASA (NNX09AH43G).

Literature Cited

Acampora, D., M. P. Postiglione, V. Avantaggiato, M. Di Bonito, F. M. Vaccarino *et al.*, 1999 Progressive impairment of developing neuroendocrine cell lineages in the hypothalamus of mice lacking the Orthopedia gene. Genes Dev. 13: 2787–2800.

Altschul, S. F., T. L. Madden, A. A. Schaffer, J. Zhang, Z. Zhang *et al.*, 1997 Gapped BLAST and PSI-BLAST: a new generation of protein database search programs. Nucleic Acids Res. 25: 3389–3402.

Altschul, S. F., J. C. Wootton, E. M. Gertz, R. Agarwala, A. Morgulis *et al.*, 2005 Protein database searches using compositionally adjusted substitution matrices. FEBS J. 272: 5101–5109.

Armstrong, J. D., M. J. Texada, R. Munjaal, D. A. Baker, and K. M. Beckingham, 2006 Gravitaxis in *Drosophila melanogaster*: a forward genetic screen. Genes Brain Behav. 5: 222–239.

Bainbridge, S. P., and M. Bownes, 1981 Staging the metamorphosis of *Drosophila melanogaster*. J. Embryol. Exp. Morphol. 66: 57–80.

Balducci-Silano, P. L., K. Suzuki, M. Ohta, J. Saito, M. Ohmori *et al.*, 1998 Regulation of major histocompatibility (MHC) class II human leukocyte antigen-DR alpha gene expression in thyrocytes by single strand binding protein-1, a transcription factor that also regulates thyrotropin receptor and MHC class I gene expression. Endocrinology 139: 2300–2313.

Bandziulis, R. J., M. S. Swanson, and G. Dreyfuss, 1989 RNA-binding proteins as developmental regulators. Genes Dev. 3: 431–437.

Bantignies, F., R. H. Goodman, and S. M. Smolik, 2000 Functional interaction between the coactivator *Drosophila* CREB-binding protein and ASH1, a member of the trithorax group of chromatin modifiers. Mol. Cell. Biol. 20: 9317–9330.

Berger, C., H. Harzer, T. R. Burkard, J. Steinmann, S. van der Horst *et al.*, 2012 FACS purification and transcriptome analysis of drosophila neural stem cells reveals a role for Klumpfuss in self-renewal. Cell Reports 2: 407–418.

Bjorum, S. M., 2006 Two genes affecting Drosophila gravitaxis. Annual Drosophila Research Conference 47: Abstract 615B.

Crown, A., D. K. Clifton, and R. A. Steiner, 2007 Neuropeptide signaling in the integration of metabolism and reproduction. Neuroendocrinology 86: 175–182.

Demerec, M., 1994 *Biology of Drosophila*. Cold Spring Harbor Laboratory Press, Cold Spring Harbor, NY.

Fontana, J. R., and S. T. Crews, 2012 Transcriptome analysis of Drosophila CNS midline cells reveals diverse peptidergic properties and a role for castor in neuronal differentiation. Dev. Biol. 372: 131–142.

Fox, R. M., C. D. Hanlon, and D. J. Andrew, 2010 The CrebA/Creb3-like transcription factors are major and direct regulators of secretory capacity. J. Cell Biol. 191: 479–492.

Goncalves, J., S. Baptista, M. V. Olesen, C. Fontes-Ribeiro, J. O. Malva *et al.*, 2012 Methamphetamine-induced changes in the mice hippocampal neuropeptide Y system: implications for memory impairment. J. Neurochem. 123: 1041–1053.

Graveley, B. R., A. N. Brooks, J. W. Carlson, M. O. Duff, J. M. Landolin *et al.*, 2011 The developmental transcriptome of *Drosophila melanogaster*. Nature 471: 473–479.

Hamanaka, Y., D. Park, P. Yin, S. P. Annangudi, T. N. Edwards *et al.*, 2010 Transcriptional orchestration of the regulated secretory pathway in neurons by the bHLH protein DIMM. Curr. Biol. 20: 9–18.

Harbison, S. T., A. H. Yamamoto, J. J. Fanara, K. K. Norga, and T. F. Mackay, 2004 Quantitative trait loci affecting starvation resistance in *Drosophila melanogaster*. Genetics 166: 1807–1823.

Hewes, R. S., A. M. Schaefer, and P. H. Taghert, 2000 The cryptocephal gene (ATF4) encodes multiple basic-leucine zipper proteins controlling molting and metamorphosis in *Drosophila*. Genetics 155: 1711–1723.

Hewes, R. S., D. Park, S. A. Gauthier, A. M. Schaefer, and P. H. Taghert, 2003 The bHLH protein Dimmed controls neuroendocrine cell differentiation in Drosophila. Development 130: 1771–1781.

Hodge, J. J., J. C. Choi, C. J. O'Kane, and L. C. Griffith, 2005 Shaw potassium channel genes in *Drosophila*. J. Neurobiol. 63: 235–254.

Huang, X. Q., and W. Miller, 1991 A time-efficient, linear-space local similarity algorithm. Adv. Appl. Math. 12: 337–357.

Jiang, N., A. S. Kolhekar, P. S. Jacobs, R. E. Mains, B. A. Eipper *et al.*, 2000 PHM is required for normal developmental transitions and for biosynthesis of secretory peptides in *Drosophila*. Dev. Biol. 226: 118–136.

Kimura, K., H. Saga, K. Hayashi, H. Obata, Y. Chimori *et al.*, 1998 c-Myc gene single-strand binding protein-1, MSSP-1, suppresses transcription of alpha-smooth muscle actin gene in chicken visceral smooth muscle cells. Nucleic Acids Res. 26: 2420–2425.

Lee, G., and J. H. Park, 2004 Hemolymph sugar homeostasis and starvation-induced hyperactivity affected by genetic manipulations of the adipokinetic hormone-encoding gene in *Drosophila melanogaster*. Genetics 167: 311–323.

Lorković, Z. J., 2012 *RNA Binding Proteins*. Eurekah, Georgetown, TX.

Luan, H., W. C. Lemon, N. C. Peabody, J. B. Pohl, P. K. Zelensky *et al.*, 2006 Functional dissection of a neuronal network required for cuticle tanning and wing expansion in *Drosophila*. J. Neurosci. 26: 573–584.

Lukacsovich, T., Z. Asztalos, W. Awano, K. Baba, S. Kondo *et al.*, 2001 Dual-tagging gene trap of novel genes in *Drosophila melanogaster*. Genetics 157: 727–742.

Luquet, S., F. A. Perez, T. S. Hnasko, and R. D. Palmiter, 2005 NPY/AgRP neurons are essential for feeding in adult mice but can be ablated in neonates. Science 310: 683–685.

Magarinos, A. M., B. S. McEwen, M. Saboureau, and P. Pevet, 2006 Rapid and reversible changes in intrahippocampal connectivity during the course of hibernation in European hamsters. Proc. Natl. Acad. Sci. USA 103: 18775–18780.

Marchler-Bauer, A., J. B. Anderson, P. F. Cherukuri, C. DeWeese-Scott, L. Y. Geer *et al.*, 2005 CDD: a conserved domain database for protein classification. Nucleic Acids Res. 33: D192–D196.

Maris, C., C. Dominguez, and F. H. Allain, 2005 The RNA recognition motif, a plastic RNA-binding platform to regulate post-transcriptional gene expression. FEBS J. 272: 2118–2131.

Matzat, L. H., R. K. Dale, N. Moshkovich, and E. P. Lei, 2012 Tissue-specific regulation of chromatin insulator function. PLoS Genet. 8: e1003069.

McShane, T. M., T. May, J. L. Miner, and D. H. Keisler, 1992 Central actions of neuropeptide-Y may provide a neuromodulatory link between nutrition and reproduction. Biol. Reprod. 46: 1151–1157.

Michaud, J. L., T. Rosenquist, N. R. May, and C. M. Fan, 1998 Development of neuroendocrine lineages requires the bHLH-PAS transcription factor SIM1. Genes Dev. 12: 3264–3275.

Milosevic, N. T., and D. Ristanovic, 2007 The Sholl analysis of neuronal cell images: semi-log or log–log method? J. Theor. Biol. 245: 130–140.

Morin, X., R. Daneman, M. Zavortink, and W. Chia, 2001 A protein trap strategy to detect GFP-tagged proteins expressed from their endogenous loci in *Drosophila*. Proc. Natl. Acad. Sci. USA 98: 15050–15055.

Nephew, B. C., R. S. Bridges, D. F. Lovelock, and E. M. Byrnes, 2009 Enhanced maternal aggression and associated changes in neuropeptide gene expression in multiparous rats. Behav. Neurosci. 123: 949–957.

Niki, T., I. Galli, H. Ariga, and S. M. Iguchi-Ariga, 2000a MSSP, a protein binding to an origin of replication in the c-myc gene, interacts with a catalytic subunit of DNA polymerase alpha and stimulates its polymerase activity. FEBS Lett. 475: 209–212.

Niki, T., S. Izumi, Y. Saegusa, T. Taira, T. Takai *et al.*, 2000b MSSP promotes ras/myc cooperative cell transforming activity by binding to c-Myc. Genes Cells 5: 127–141.

Nomura, J., K. Matsumoto, S. M. Iguchi-Ariga, and H. Ariga, 2005 Positive regulation of Fas gene expression by MSSP and abrogation of Fas-mediated apoptosis induction in MSSP-deficient mice. Exp. Cell Res. 305: 324–332.

Park, D., O. T. Shafer, S. P. Shepherd, H. Suh, J. S. Trigg *et al.*, 2008 The *Drosophila* basic helix–loop–helix protein DIMMED directly activates PHM, a gene encoding a neuropeptide-amidating enzyme. Mol. Cell. Biol. 28: 410–421.

Park, J. H., A. J. Schroeder, C. Helfrich-Forster, F. R. Jackson, and J. Ewer, 2003 Targeted ablation of CCAP neuropeptide-containing neurons of Drosophila causes specific defects in execution and circadian timing of ecdysis behavior. Development 130: 2645–2656.

Park, Y., V. Filippov, S. S. Gill, and M. E. Adams, 2002 Deletion of the ecdysis-triggering hormone gene leads to lethal ecdysis deficiency. Development 129: 493–503.

Peabody, N. C., F. Diao, H. Luan, H. Wang, E. M. Dewey *et al.*, 2008 Bursicon functions within the *Drosophila* CNS to modulate wing expansion behavior, hormone secretion, and cell death. J. Neurosci. 28: 14379–14391.

Reis, T., M. R. Van Gilst, and I. K. Hariharan, 2010 A buoyancy-based screen of *Drosophila* larvae for fat-storage mutants reveals a role for Sir2 in coupling fat storage to nutrient availability. PLoS Genet. 6: e1001206.

Ryder, E., M. Ashburner, R. Bautista-Llacer, J. Drummond, J. Webster *et al.*, 2007 The DrosDel deletion collection: a *Drosophila* genomewide chromosomal deficiency resource. Genetics 177: 615–629.

Seki, Y., J. Rybak, D. Wicher, S. Sachse, and B. S. Hansson, 2010 Physiological and morphological characterization of local interneurons in the *Drosophila* antennal lobe. J. Neurophysiol. 104: 1007–1019.

Shakiryanova, D., A. Tully, R. S. Hewes, D. L. Deitcher, and E. S. Levitan, 2005 Activity-dependent liberation of synaptic neuropeptide vesicles. Nat. Neurosci. 8: 173–178.

Siekhaus, D. E., and R. S. Fuller, 1999 A role for amontillado, the *Drosophila* homolog of the neuropeptide precursor processing protease PC2, in triggering hatching behavior. J. Neurosci. 19: 6942–6954.

Slaidina, M., R. Delanoue, S. Gronke, L. Partridge, and P. Leopold, 2009 A *Drosophila* insulin-like peptide promotes growth during nonfeeding states. Dev. Cell 17: 874–884.

Tamura, K., D. Peterson, N. Peterson, G. Stecher, M. Nei *et al.*, 2011 MEGA5: molecular evolutionary genetics analysis using maximum likelihood, evolutionary distance, and maximum parsimony methods. Mol. Biol. Evol. 28: 2731–2739.

Tan, C. K., H. Lovlie, E. Greenway, S. F. Goodwin, T. Pizzari *et al.*, 2013 Sex-specific responses to sexual familiarity, and the role of olfaction in *Drosophila*. Proc. Biol. Sci. 280: 20131691.

Wang, H., X. Chen, T. He, Y. Zhou, and H. Luo, 2013 Evidence for tissue-specific Jak/STAT target genes in *Drosophila* optic lobe development. Genetics 195: 1291–1306.

Yeh, E., K. Gustafson, and G. L. Boulianne, 1995 Green fluorescent protein as a vital marker and reporter of gene expression in *Drosophila*. Proc. Natl. Acad. Sci. USA 92: 7036–7040.

Zhao, T., T. Gu, H. C. Rice, K. L. McAdams, K. M. Roark *et al.*, 2008 A Drosophila gain-of-function screen for candidate genes involved in steroid-dependent neuroendocrine cell remodeling. Genetics 178: 883–901.

Communicating editor: H. J. Bellen

GENETICS

Supporting Information
http://www.genetics.org/lookup/suppl/doi:10.1534/genetics.114.166181/-/DC1

Neuronal Remodeling During Metamorphosis Is Regulated by the *alan shepard* (*shep*) Gene in *Drosophila melanogaster*

Dahong Chen, Chunjing Qu, Sonia M. Bjorum, Kathleen M. Beckingham, and Randall S. Hewes

DOI: 10.1534/genetics.114.166181

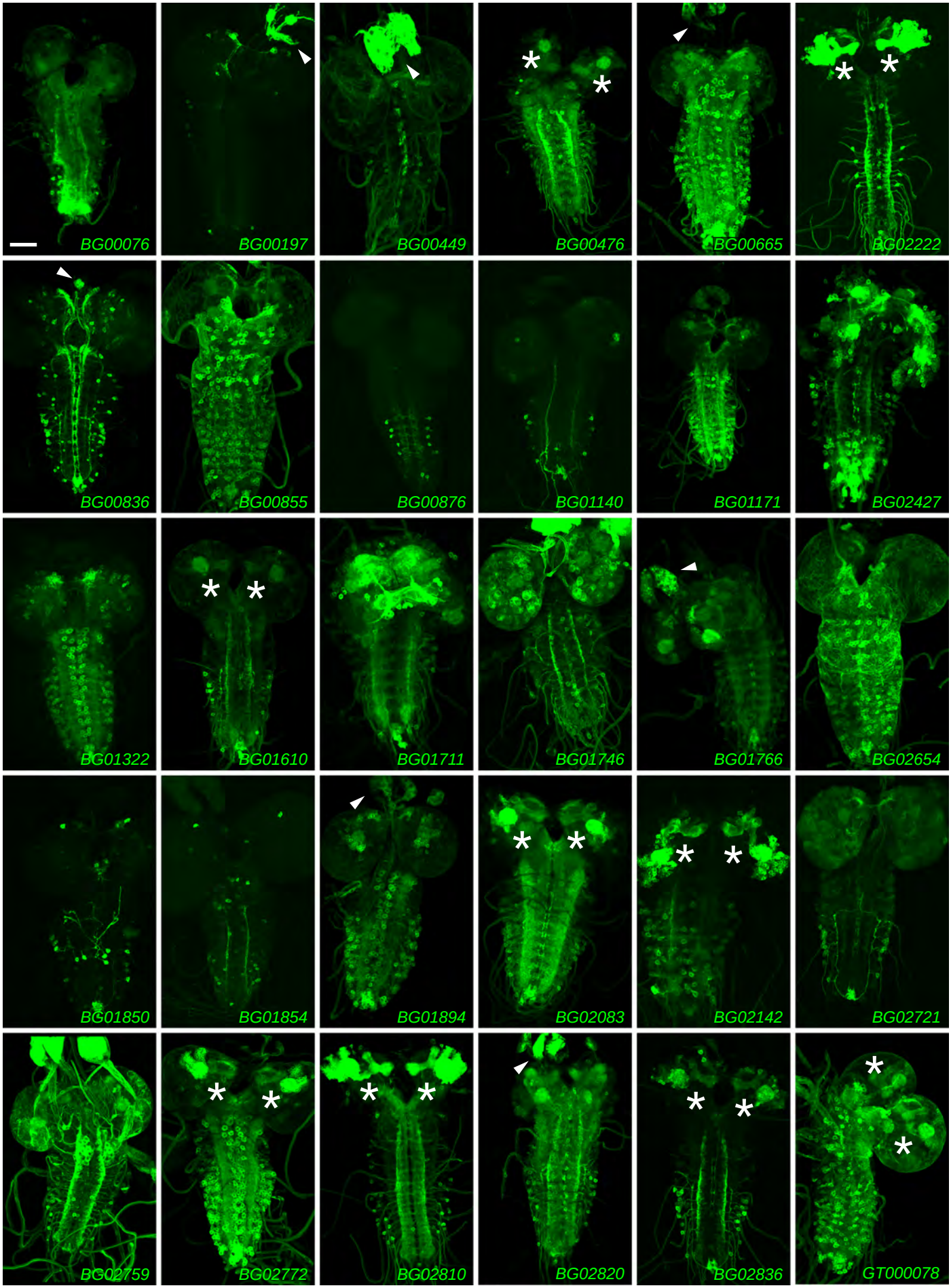

Figure S1 Reporter gene expression patterns for 30 insertions with expression in neurons. Each line was crossed to *UAS-mCD8::GFP* prior to isolation of the CNS at the wandering 3rd instar larval stage, and representative confocal z-series projections of fixed tissues are shown. Arrowheads indicate expression in the ring gland, and asterisks denote expression in the mushroom bodies. Scale bar: 50µm.

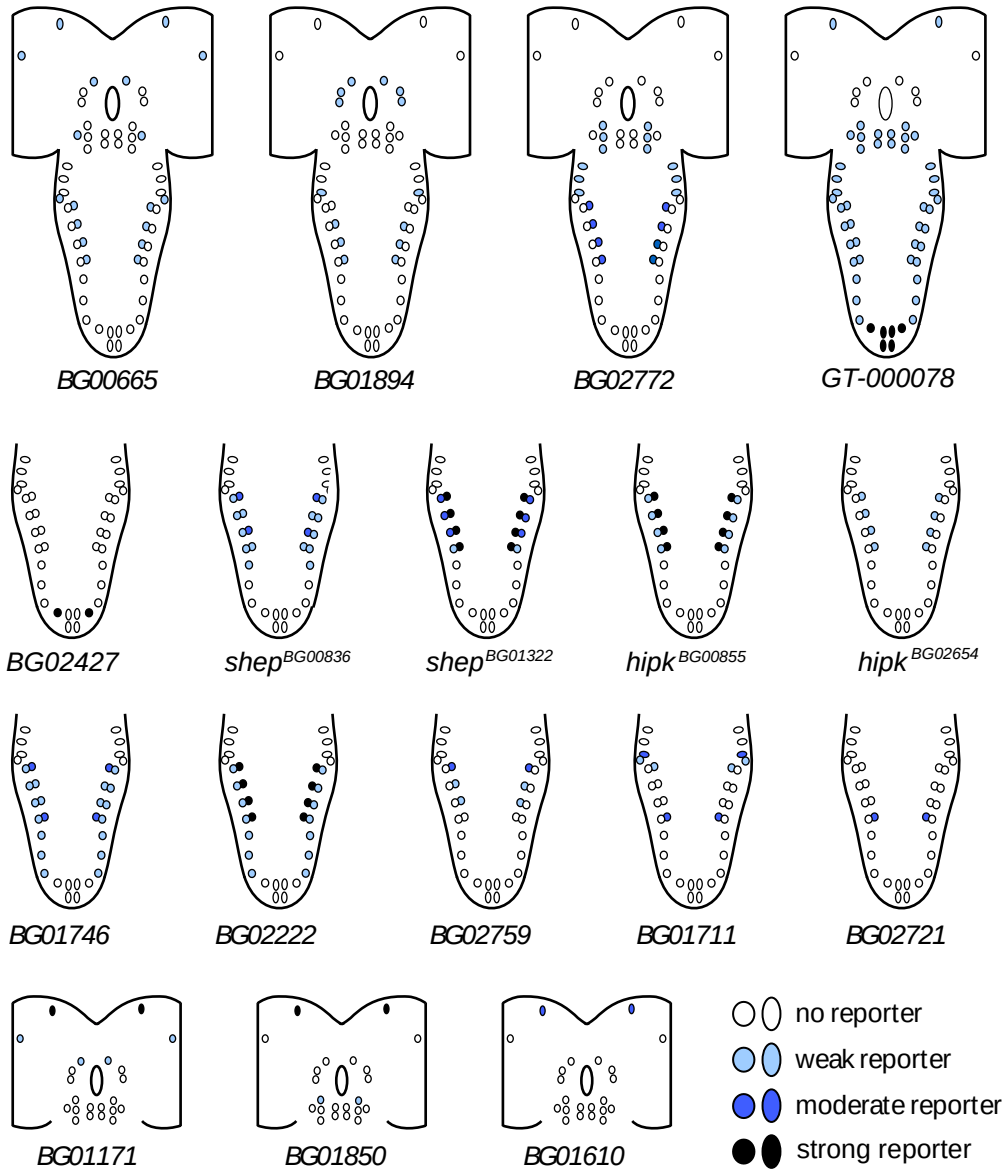

Figure S2 Patterns of splice-trap reporter gene expression in CCAP neurons in the wandering 3rd instar larval CNS. We found 17 insertions that drove expression in CCAP neurons, which are indicated with circles on the schematic CNS diagrams. The relative intensities of GFP reporter expression (mCD8::GFP, subjective scale) are indicated with different colors, and CCAP neurons with no detectable expression of the reporter are indicated with open circles. If there was no reporter expression in the brain lobes or ventral nerve cord, those regions of the CNS are not shown.

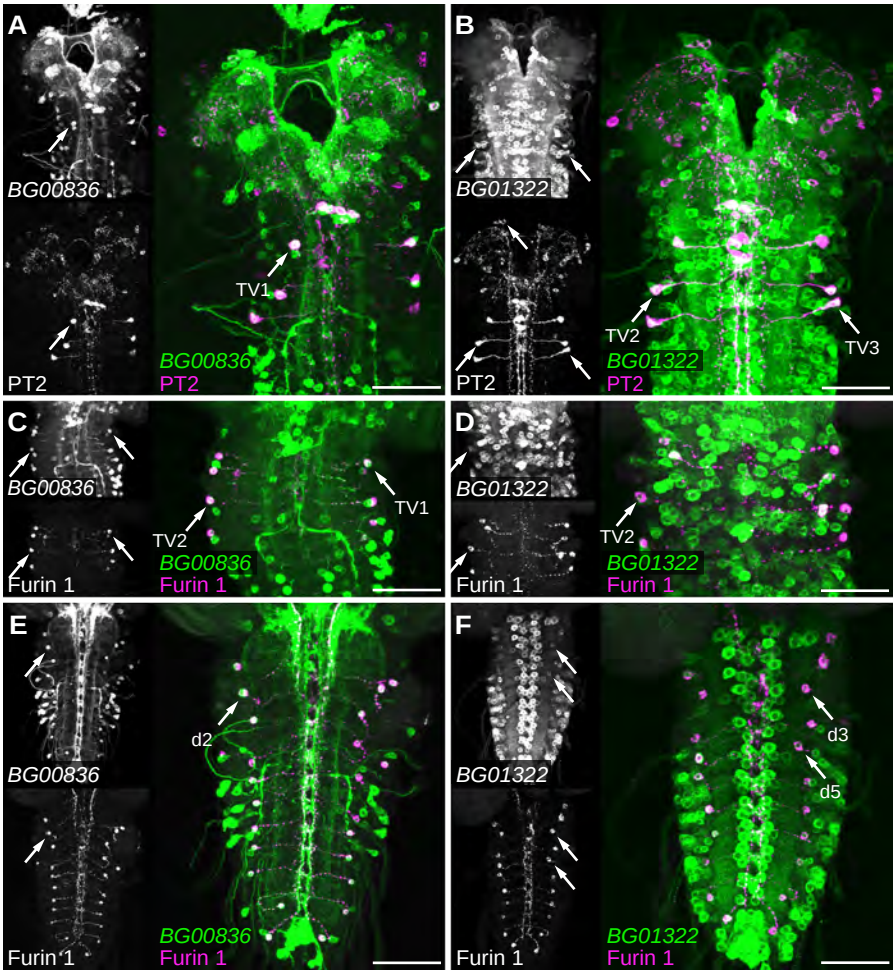

Figure S3 Reporter gene expression for the two *shep* splice-trap insertions, *BG00836* and *BG01322*, in multiple types of peptidergic neurons. (A-B) Co-localization of immunostaining with the PT2 antiserum (magenta) and mCD8::GFP reporter expression driven by *BG00836* (panel A) and *BG01322* (panel B). (C-F) Co-localization of anti-Furin 1 immunostaining (magenta) and mCD8::GFP reporter expression driven by *BG00836* (panels C and E) and *BG01322* (panels D and F). Panels C and D are ventral views of a portion of the ventral nerve cord, and panels E and F are dorsal views. Arrows: examples of colocalization of the immunosignal and reporter gene expression. Scale bars: 50 µm.

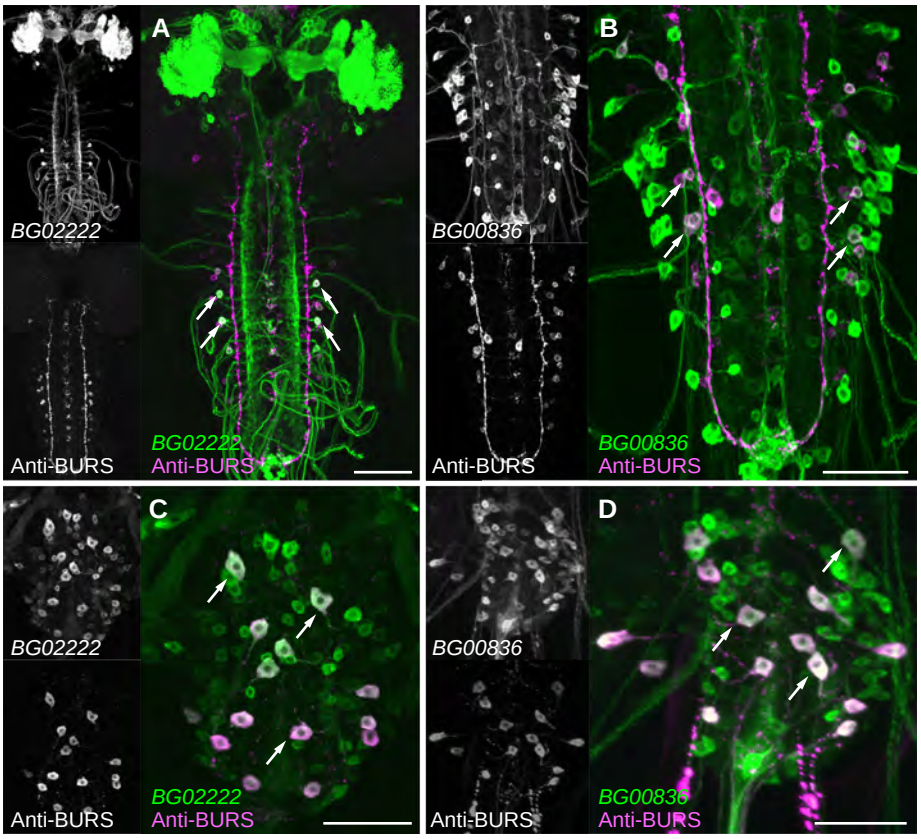

Figure S4 Selected splice-trap expression patterns that contained bursicon neurons. (A-B) Co-localization of immunostaining with an anti-BURS antiserum (magenta) and mCD8::GFP reporter expression (green) driven by *BG02222* (panel A) and *BG00836* (panel B) in wandering 3rd instar larvae. (C-D) At the P14 pharate adult stage, both *BG02222* and *BG00836* drove reporter expression in all 14 bursicon neurons in the abdominal ganglia. Arrows, examples of abdominal bursicon neurons with co-localization of the two markers. Scale bars: 50 μm.

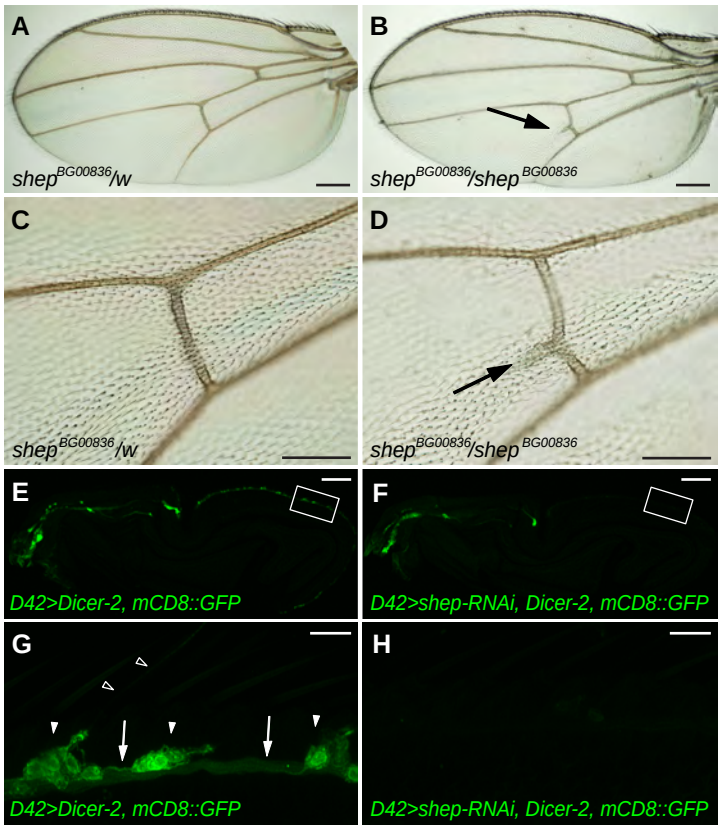

Figure S5 Loss of wing sensory neurons and appearance of ectopic wing veins following loss of *shep*. (A-D) 40% (23 out of 57) *shep*^{BG00836} homozygotes had an ectopic vein on the posterior crossvein (arrows) that was not found in *shep*^{BG00836}*/w* control flies. Panels C-D are higher magnification views of the region containing the posterior crossvein. Scale bars: A and B, 200 µm; C and D, 100 µm. (E) At the P14 pharate adult stage, sensory neurons on the wings of *D42>Dicer-2, mCD8::GFP* flies had proximal neurite projections. (F) In *shep* RNAi animals (*D42>shep-RNAi, Dicer-2, mCD8::GFP*), the proximal projections and most sensory neuron somata were absent. Scale bars: 100 µm. (G-H) Higher magnification views of the developing wing border in the highlighted box in panel E and F. Arrows, sensory neurons; Arrowheads, neurite projections of the sensory neurons; Open arrowheads, bristle neurites. Scale bars: 10 µm.

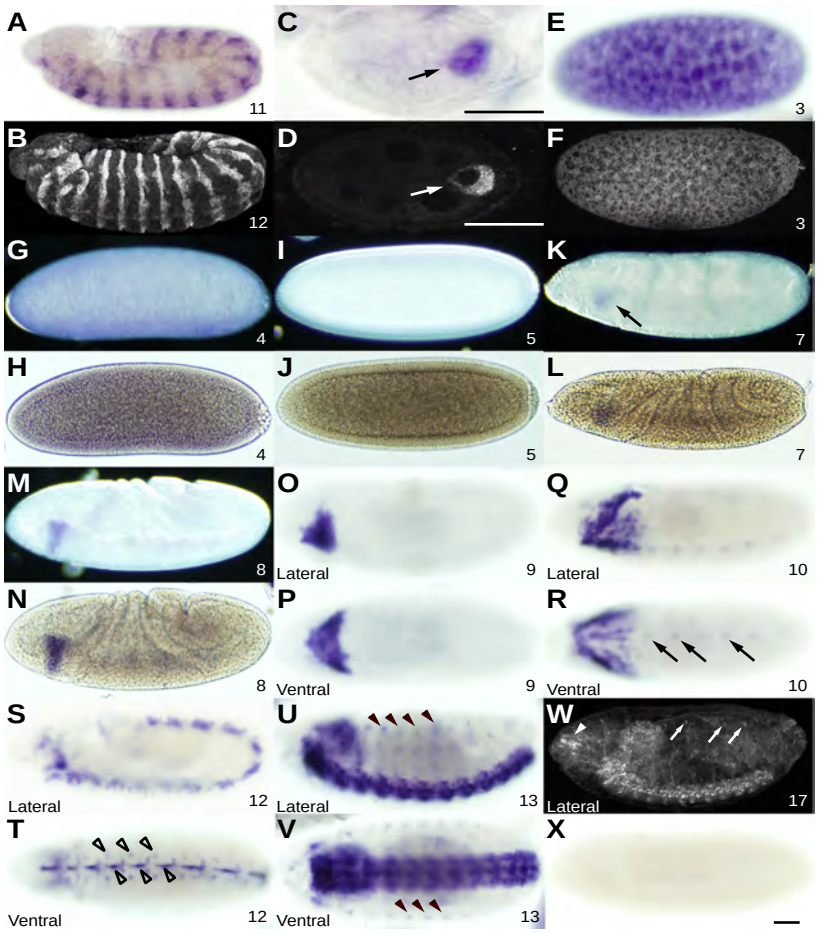

Figure S6 Embryonic *shep* mRNA and SHEP protein expression patterns. (A-B) Ectopic expression of *shep* in stage 11-12 *engrailed-Gal4/UAS-shep* embryos was detected by *in situ* hybridization (A) and immunostaining (B) with an anti-SHEP antiserum. (C-F) Expression of *shep* was detected in oocytes (arrows in panels C-D) in the ovaries of P14 stage pharate adult females and in syncytial blastoderm embryos (panels E-F) by *in situ* hybridization (blue) and immunostaining with antibodies to SHEP (gray). (G-N) Expression of *shep* in early embryonic stages detected by *in situ* hybridization. Each top-bottom pair of images shows signals from the same embryo with dark field and köhler illumination. Zygotic *shep* was first detected at stage 7 in the pro-cephalic neurogenic region (arrow, panel K). (O-V) In later embryonic stages, the expression of *shep* expanded to include the entire central and peripheral nervous systems. Each top-bottom pair of images are lateral (top) and ventral (bottom) views of the same embryos. Arrows, putative mesectoderm; open arrowheads, ventral neurogenic region; arrowheads, peripheral nervous system. (W) Anti-SHEP immunostaining produced labeling in the CNS, PNS (arrows), and the antennomaxillary complex and labral sensory complex (arrowhead). (X) Control *in situ* hybridization with the sense probe in an *Oregon R* embryo. The embryonic stage is indicated in the lower right corner of each panel. Scale bars: (C, D), 25 μm; (all other panels), 50 μm.

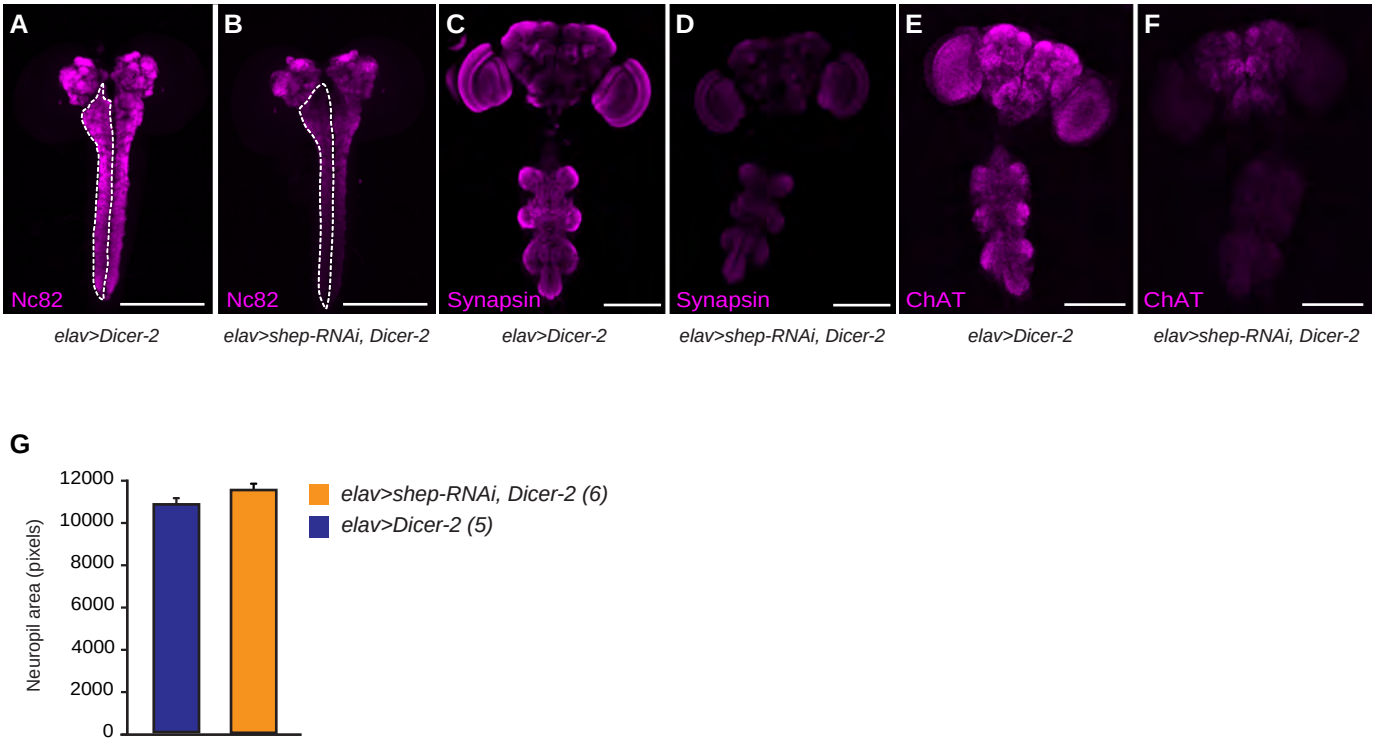

Figure S7 Loss of *shep* led to reduced levels of multiple presynaptic markers in the larval and pharate adult CNS. (A-B) Anti-nc82 immunostaining for the active zone protein Bruchpilot in wandering 3rd instar *elav>shep-RNAi, Dicer-2* larvae displayed lower signal intensity (panel B) than in *elav>Dicer-2* control larvae (panel A). (C-F) Immunostaining in P14 pharate adult CNS for Synapsin and Choline acetyltransferase (ChAT) revealed lower levels of both presynaptic markers in *shep* RNAi animals (D, F) than in *elav>Dicer-2* controls (C, E). Scale bars: 200 µm. (G) Quantification of neuropil area for the anti-nc82 immunostaining in wandering 3rd instar larvae. The ventral nerve cord neuropil area (dashed lines, panels A and B) was unchanged in *elav>shep-RNAi, Dicer-2* animals at the wandering 3rd instar stage (P=0.143, Student's t-test).

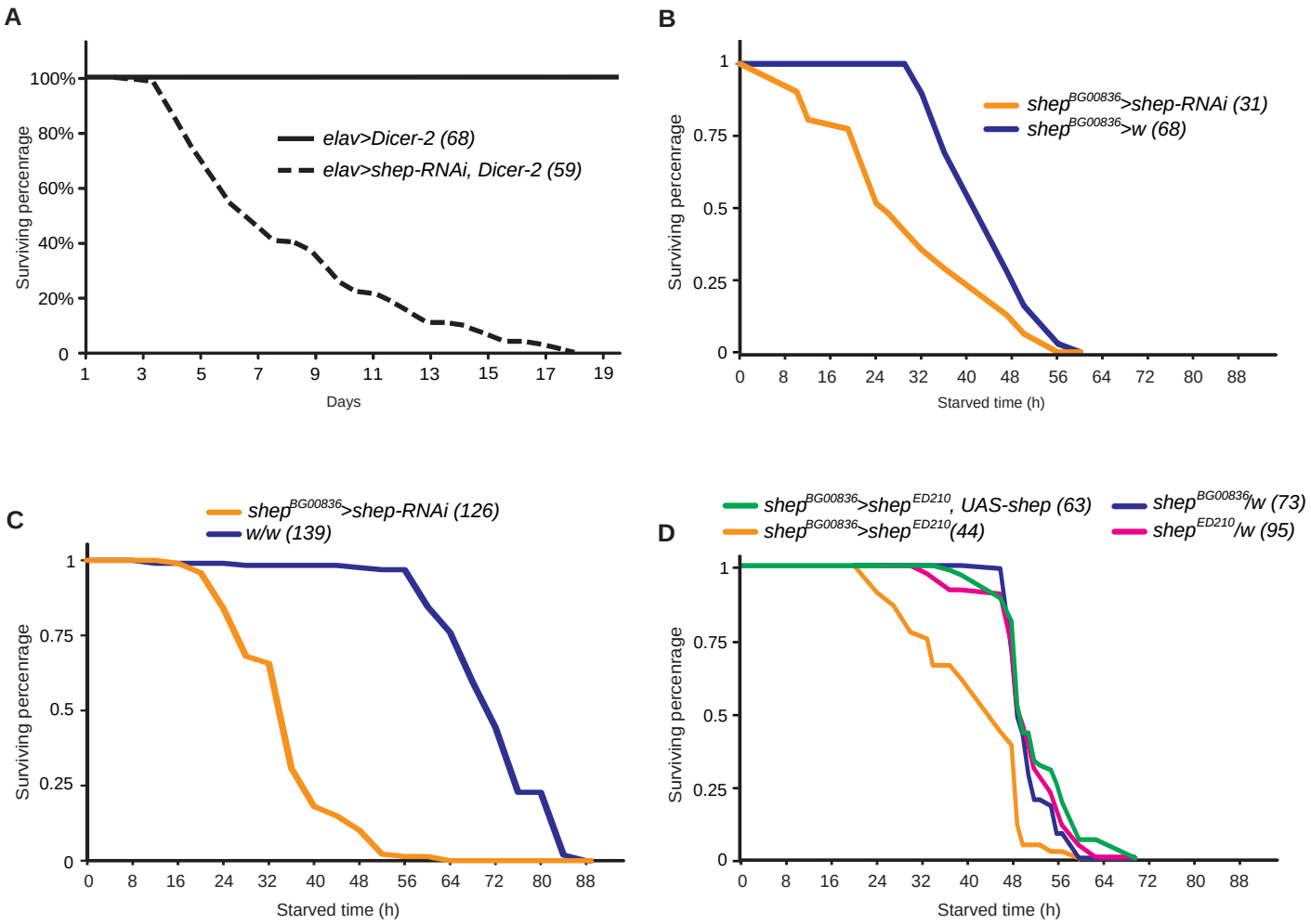

Figure S8 Loss of *shep* resulted in reduced life span. (A) Pan-neuronal *shep* RNAi led to shorter life span. The running percentage of surviving adults was plotted for *elav>shep-RNAi, Dicer-2* and *elav>Dicer-2* adult flies on regular food. (B-D) Reduced starvation resistance was detected in multiple *shep* mutants. Cumulative survival under starvation conditions was calculated (see methods) for $shep^{BG00836}$ *>shep-RNAi,* $shep^{BG00836}$ homozygotes, $shep^{BG00836}/shep^{ED210}$ mutants, and $shep^{BG00836}/shep^{ED210}$*, UAS-shep* rescue flies. In each panel, the *shep* loss-of-function genotype is labeled in orange. The results for *shep* heterozygotes are shown in blue and magenta, and the results for flies rescued with *UAS-shep* are shown in green. Sample sizes are listed in parentheses following each genotype.

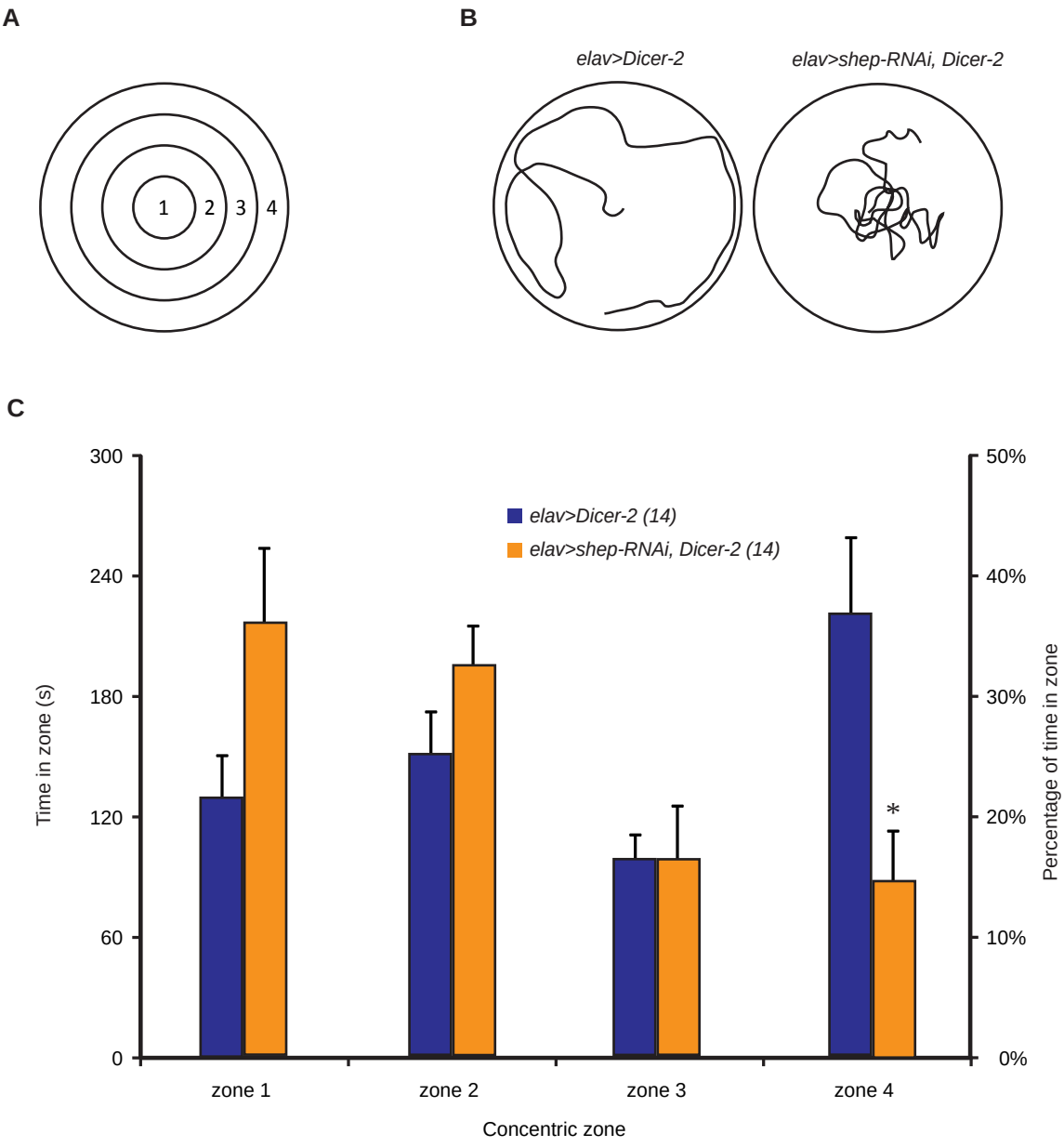

Figure S9 Pan-neuronal loss of *shep* produced larvae that remained near the center of apple-juice plates during locomotor behavior assays. (A) Apple juice-agarose plates were placed on a grid of concentric circles that defined four zones from the center to the periphery. (B) Representative 10-minute crawling trails for *elav>Dicer-2* and *elav>shep-RNAi, Dicer-2* wandering 3rd instar larvae. (C) The percentage of time spent by *elav> Dicer-2* and *elav>shep-RNAi, Dicer-2* larvae in each of the four concentric zones. The number of animals for each genotype is indicated in parentheses. *P<0.05; Separate Student's *t*-tests with Bonferroni correction were performed for each zone.

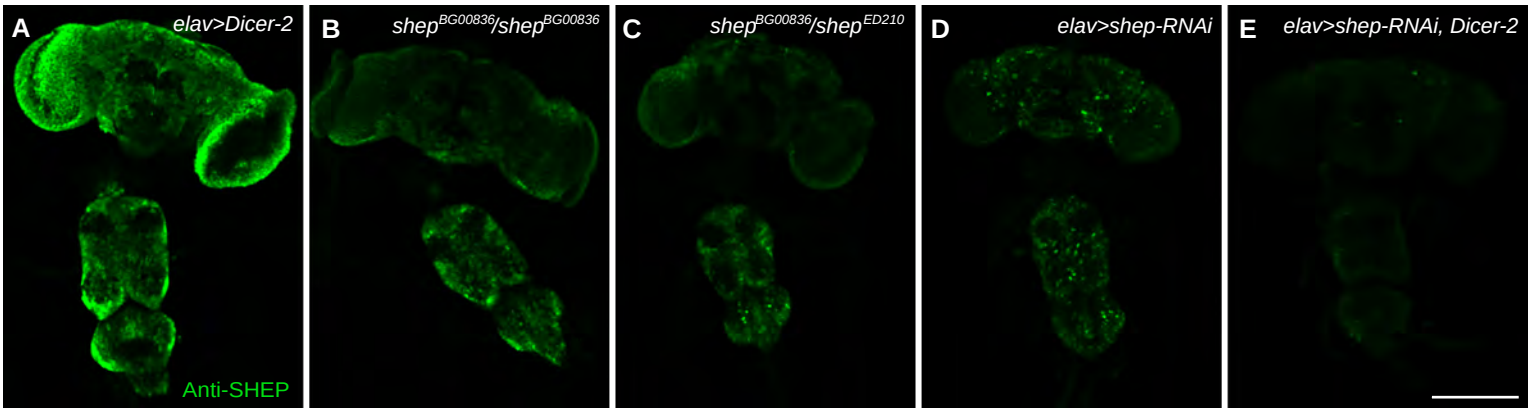

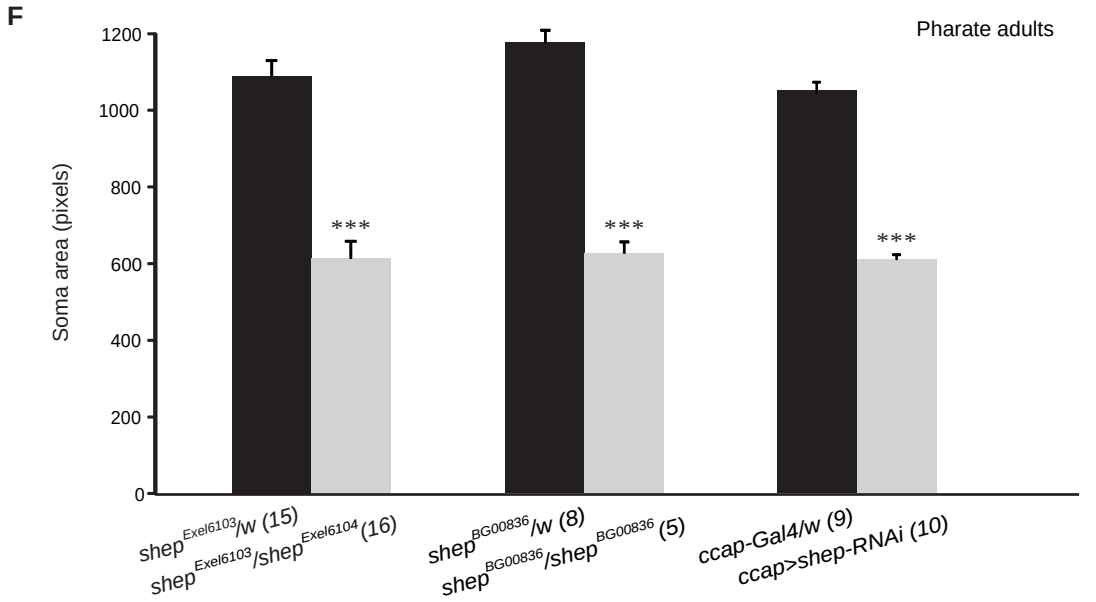

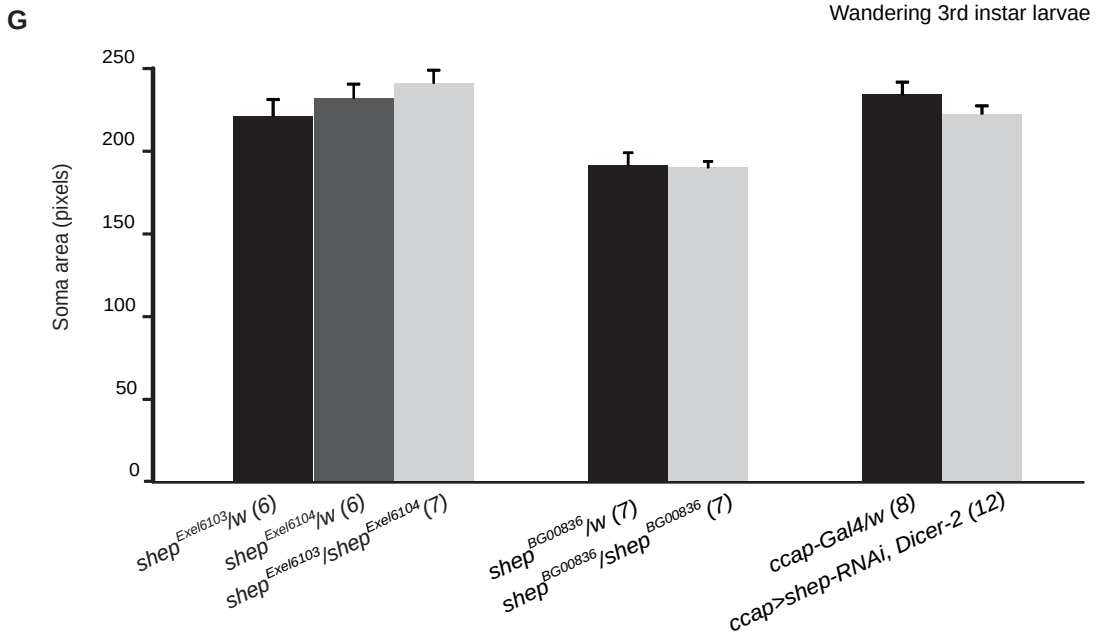

Figure S10 Loss of SHEP resulted in smaller bursicon neurons in P14 stage pharate adults but not in wandering 3rd instar larvae. (A-E) Anti-SHEP immunostaining of *shep* loss-of-function mutants at the P14 pharate adult stage. Lower SHEP levels were observed in all of the *shep* mutant backgrounds, but *elav>shep-RNAi, Dicer-2* displayed the greatest reduction of SHEP levels in the CNS. (F) In P14 stage pharate adults, we observed reduced bursicon neuron soma areas in hypomorphic *shep* mutant backgrounds, which included $shep^{Exel6103}/shep^{Exel6104}$, $shep^{BG00836}$ homozygotes, and *ccap>shep-RNAi*. (G) Bursicon neuron soma areas were unaffected in wandering 3rd larval instar *shep* mutants. The mutant backgrounds included *ccap>shep-RNAi, Dicer-2*, which was the strongest *shep* loss-of-function genotype, as judged by the impacts on branching in the peripheral axon arbor (Figure S11). The number of animals for each genotype is indicated in parentheses. **P*<0.05, ***P*<0.01, ****P*<0.001, Student's *t*-test. Scale bar: 200 µm.

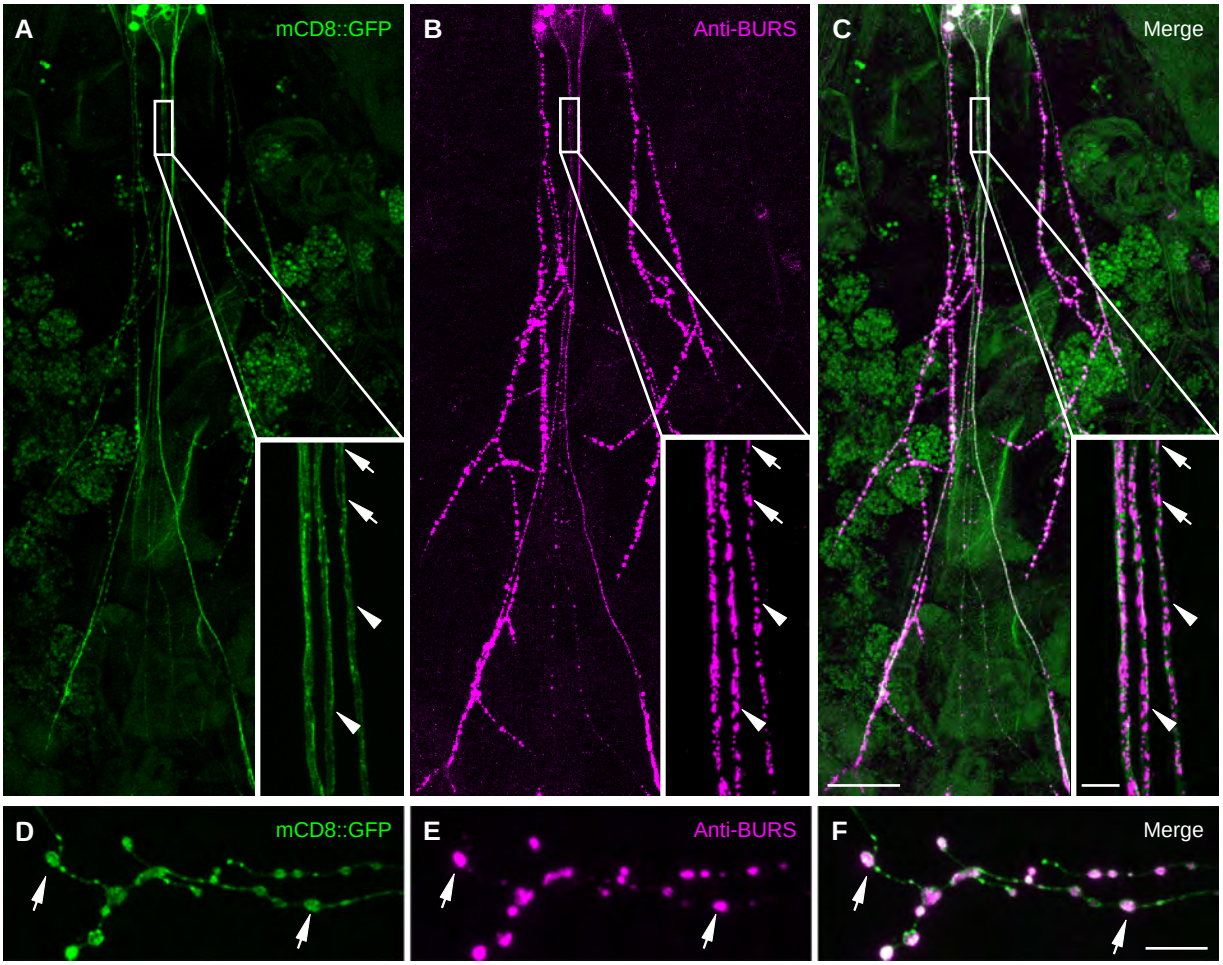

Figure S11 Bursicon neuron peripheral axon projections and synaptic terminals were visualized by anti-BURS immunostaining or genetic labeling with the membrane-localized fusion protein, mCD8::GFP. (A-C) Peripheral axons in the abdominal nerves of a *ccap>shep-RNAi, Dicer-2, mCD8::GFP* P14 stage pharate adult. Although the anti-BURS immunostaining (magenta) is more restricted to boutons than the mCD8::GFP labeling (green), each axon in the nerve can be clearly resolved at lower magnification (panels A-C), which captures most of the peripheral axon arbor, and at higher magnification (insets; region of the abdominal nerve trunk indicated by the white boxes in panels A-C). Within the abdominal nerve trunk, there is much less bursicon accumulation than in the distal boutons, but anti-BURS immunostaining still permits the visualization of each axon. Arrows, boutons; arrowheads, axons. Scale bars: A-C, 100 µm; insets, 5 µm. (D-F) Labeling of the bursicon neuron terminals on muscles 12-13 of the 2nd abdominal segment with mCD8::GFP (green) and anti-BURS immunostaining (magenta) in *ccap>shep-RNAi, Dicer-2, mCD8::GFP* wandering 3rd instar larvae. Arrows, boutons. Scale bar: 10 µm.

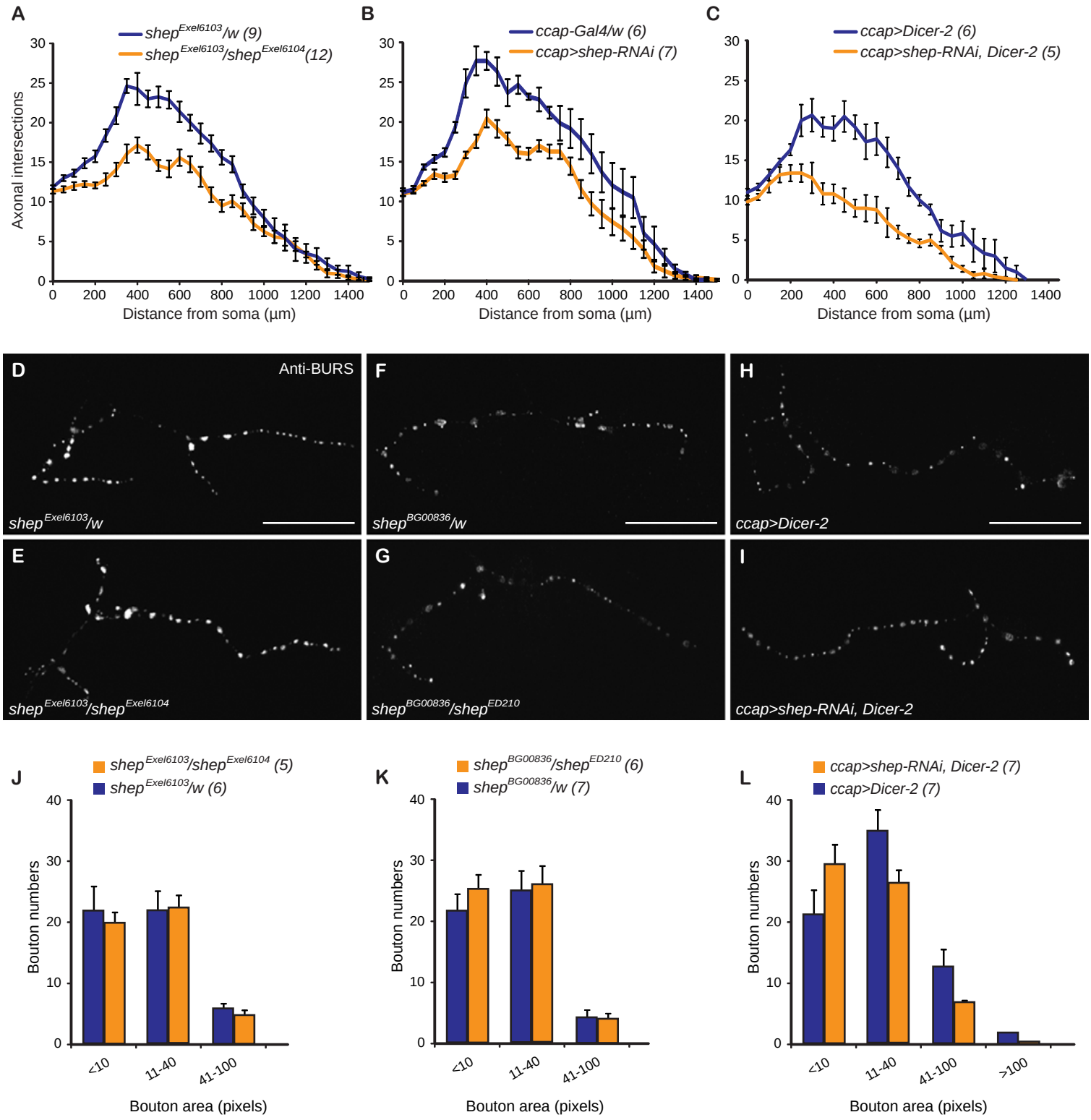

Figure S12 *shep* promoted outgrowth of the peripheral projections of the bursicon neurons during metamorphosis. (A-C) Sholl analysis on the peripheral projections of P14 stage pharate adult bursicon neurons. For this analysis, we counted the number of axon intersections with nested, concentric rings, each with a 50 µm increase in radius from the next smallest ring. Sample sizes are listed in parentheses following each genotype. (D-I) In wandering 3rd instar larvae, the morphology of the neuromuscular junctions (NMJ) of the hypomorphic mutants *shep*^{Exel6103}/*shep*^{Exel6104} (E), *shep*^{BG00836}/*shep*^{ED210}(G), and *ccap>shep-RNAi, Dicer-2* (I) was similar to the morphology of the respective hemizygous controls (D, F, and H). (J-L) Binned counts of wandering 3rd instar larval NMJ boutons within size classes for *shep* loss-of-function animals. Sample sizes are listed in parentheses. Two-way ANOVAs, P=0.452479 (panel J), P=0.597591 (panel K), and P=0.271019 (panel L). Scale bars: 100 µm.

Files S1-S5

Available for download as .avi files at http://www.genetics.org/lookup/suppl/doi:10.1534/genetics.114.166181/-/DC1

File S1 Mounting of an *Oregon R* female by an *Oregon R* virgin male. The male mounted the female shortly after copulation started, and the female extended her wings to accept the male.

File S2 Kicking of an *Oregon R* male by a $shep^{BG00836}/shep^{ED210}$ virgin female after the onset of copulation. The female continued to kick the male during copulation and did not extend her wings to accept mounting by the male.

File S3 Three-leg grooming by a $shep^{BG00836}/shep^{ED210}$ female immediately after copulation was completed. The predominant grooming pattern involved only the legs, with the two metathoracic legs rubbed together with one of the mesothoracic legs (Figure 5). Correspondingly, the proportion of time spent grooming the wings and abdomen was reduced.

File S4 Two-leg grooming of an *Oregon R* female immediately after copulation. Grooming of the wings and abdomen was performed with the two metathoracic legs.

File S5 Expulsion of what appears to be seminal fluid and the mating plug by a $shep^{BG00836}/shep^{ED210}$ female immediately after copulation. The mated $shep^{BG00836}/shep^{ED210}$ female groomed with three legs and then expelled material after ovipositor extrusion. There is a one-minute pause in the video, during which the fluid was first visible after repetitive ovipositor extrusion.